TECTONICS, VOL. 5, NO. 1, PAGES 65-94, FEBRUARY 1986

STRUCTURAL HISTORY OF CONTINENTAL VOLCANIC ARC ROCKS, EASTERN SIERRA NEVADA, CALIFORNIA: A CASE FOR EXTENSIONAL TECTONICS

Othmar T. Tobisch

Earth Science Department, Applied Science Building, University of California Santa Cruz

Jason B. Saleeby

Division of Geological and Planetary Sciences, California Institute of Technology, Pasadena

Richard S. Fiske

National Museum of Natural History Smithsonian Institution Washington, D. C.

Abstract. Mesozoic metavolcanic rocks forming part of the continental volcanic arc along the eastern Sierra Nevada near Mt. Goddard and in the Ritter Range show a complex history related to extensional tectonics. The rocks comprise a thick section of tuffs, breccias, lava flows, sills, and ash-flow tuffs deposited in a subaerial to subaqueous environment, with some subvolcanic sill-like plutons. Pb/U ages of the rocks in the Mt. Goddard area range from ca. 130-160 Ma, while rocks in the Ritter Range have a somewhat wider age range as reported previously. Repetition of the section occurs by faulting, and with the exception of parts of the mid-Cretaceous Minarets Caldera, all the volcanic rocks show a regional slaty cleavage which was subsequently crenulated and/or folded locally. The first cleavage has well-developed stretching lineations, and does not appear to have been associated with significant folding. Finite strain measurements show considerable variation both in magnitude and symmetry. The Mt. Goddard rocks, however, tend to show slightly higher overall strain magnitude and greater constrictional component than the Ritter Range for rocks of comparable age. Calculations based on the strain data suggest the Mt. Goddard section has been thinned by about 50% normal to bedding, much as that documented previously for rocks in the Ritter Range. Deformation within this part of the continental arc was originally thought to have formed by regional compression during the late Jurassic (Nevadan) orogeny. However, our study indicates that (1) parts of the deformed volcanic section are younger than late Jurassic, (2) Nevadan-age breaks in deposition are not present, (3) large-scale folds expected during a regional compression event are not common, and (4) the beds were tilted to a high dip prior to internal deformation. An extensional model is proposed in which beds were rotated to high tilts early in the deformation as a result of listric normal faulting. This normal faulting is thought to have occurred above a regional tumescence related to voluminous magmatism at depth, with preservation of the steeply tilted Goddard and Ritter sections being facilitated by their downward transport along the margins of rising plutons. Flattening and steeply plunging constrictional fabrics superimposed on the tilted sections are related to strain induced by high-level inflation of magma chambers and downward return flow of the

Paper number 5T0776
0278-7407/86/005T-0776$10.00

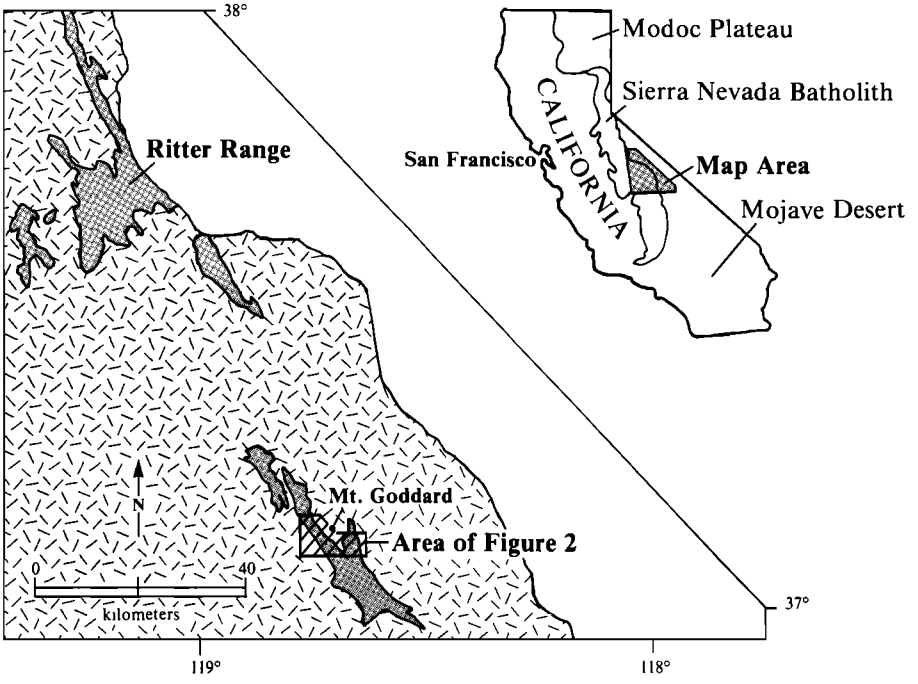

Fig. 1. Location map of the study area, which contains a 120 km long section of the continental volcanic arc in the eastern Sierra Nevada, California. Shaded pattern indicates predominantly Mesozoic age metavolcanic rocks; igneous pattern indicates predominantly Mesozoic plutonic rocks; clear pattern indicates area of predominantly Holocene age rocks.

keellike pendants. The main tectonic fabric shown by the continental volcanic arc rocks in the eastern Sierra Nevada is largely of Cretaceous age, rather than Jurassic (Nevadan) as originally supposed. In addition, the deformation, both rotation of beds and subsequent tectonite fabric, appears to be genetically related to the dynamic evolution of the magmatic arc, and not the result of an externally imposed tectonic event.

INTRODUCTION

General

Mesozoic continental volcanic arc rocks of the eastern Sierra Nevada extend for at least 500 km from the Modoc Plateau of northern California to the Mojave Desert in the south (insert, Figure 1). Over the past several years, we have been studying the structural genesis of these rocks in order to address whether deformation within the arc was due largely to (1) its collision with exotic terranes accreted to the continental margin, or (2) inherent in the dynamic evolution of magmatic arcs, or (3) some combination of both. The ultimate answer to such questions may be long in coming, but our present data allows us to analyze the nature of deformation from parts of this arc and discuss certain aspects of its structural genesis.

Previous Work

Much mapping has been carried out in the Mesozoic continental arc rocks of the eastern Sierra Nevada, largely in connection with quadrangle mapping by the U.S. Geological Survey [e.g., Moore, 1963; Rinehart and Ross, 1964; Huber and Rinehart, 1965; Bateman, 1965; Bateman and Moore, 1965]. This work has served as a firm basis for subsequent topical studies [e.g., Kistler, 1966; Brook, 1977; Nokleberg, 1981; Nokleberg and Kistler, 1980; Kistler and Swanson, 1981; Tobisch and Fiske, 1982; Schweickert et al., 1984a]. In spite of these numerous investigations, the nature and timing of deformation along the length of the arc is still poorly known, and the quantification of cumulative strains and

how these may vary with age in different parts of the arc are only just beginning to be understood [Tobisch et al., 1977; Tobisch and Fiske, 1982; this report].

The structural history and strains in Mesozoic volcanic arc rocks of the Ritter Range (Figure 1) have been studied in detail by various workers [Kistler, 1966; Tobisch et al., 1977; Fiske and Tobisch, 1978; Tobisch and Fiske, 1982]. Another large enclave of comparable rocks occurs some 85 km to the south in the Mt. Goddard region (Figure 1). Since the initial mapping of these rocks by Bateman [1965] and Bateman and Moore [1965], some work has been done [DuBray, 1977], but the structural character of the rocks has not been studied in detail. The present work investigates the structural history and strains found in rocks of the Mt. Goddard region. We then compare these data to structures which occur in the Mt. Ritter area and consider the implications concerning the broader structural evolution of this part of the arc.

GEOLOGIC SETTING

Rock Types and Depositional Environment

The volcanic section in the Mt. Goddard area is mostly volcaniclastic consisting largely of fine-grained tuffs, lithic and rarely accretionary lapilli tuffs, tuff-breccias, ash flow tuffs, mafic and felsic lava flows, lime-rich tuffs, and rare limestone. Thin Mn-rich zones bearing piemontite are present locally, and felsic sills are common in parts of the section (Plate 1; cf. also Bateman and Moore [1965]). In this paper, we refer to the rocks by their volcanic terminology, although they have been subject to regional metamorphism and penetrative deformation.

Units 1-8 (Plate 1) show depositional features of both subaqueous (graded bedding, cross-bedding, limestone) and subaerial conditions (basalt flows lack pillows, presence of red, hematite-bearing beds, lack of doubly graded sequences of lapilli tuff and tuff [Fiske and Matsuda, 1964; Fiske, 1969]. The environment of deposition of this part of the section is interpreted as being one in which the rate of deposition was more or less equal to the rate of subsidence, giving rise to periods of alternating shallow subaqueous and low-lying subaerial conditions. Units 9-12, however, are characterized by rapidly changing lateral facies, complex primary geometry, the presence of accretionary lapilli, and an absence of limestone. In addition, unit 12 shows a complex geometry between a coarse breccia and ash flow tuff, highly reminiscent of the caldera collapse unit described from the Ritter Range [Fiske et al., 1977; Fiske and Tobisch, 1978]. From these and previously mentioned observations, we conclude that units 9-12 (Plate 1) have been deposited for the most part under subaerial conditions, and that unit 12 may represent massive wall-rock slumping associated with ash flow eruption in a caldera environment.

Stratigraphy

As shown in Plate 1, the predominant dip of bedding in all units is to the west. Sedimentary structures such as current bedding, graded bedding, ripple marks, channeling, and rip-up clasts also indicate that tops face to the west. Based on field relationships and radiometric data, we have divided the volcanic section into three age groups (Figure 2): an older section represented by units 4-8 with an age of 160 Ma, an intermediate section represented by units 9-12 with an age of 143 Ma, and a younger section represented by units 1-2 with an age of 130-135 Ma. As can be seen from Figure 2, the older section is sandwiched between the intermediate and younger sections. The exact locations of the boundaries between these three groups are in part tentative due to the lack of detailed age control. The ages of units 1,6, and 8-12, however, are either precisely known or can be tightly constrained by known ages of intrusive bodies which have been dated (Plate 1; Table 2). In the northern part of the area, units 2 and 4 are separated by a laminated phyllitic schist. This schist (unit 3, northern sector) is an intensely deformed, commonly platy rock which has been subsequently subjected to kinking and locally intense secondary deformation, and probably represents a bedding parallel fault separating units 2 and 4. While the strongly laminated nature of the deformed zone diminishes to the south, the high strains which characterize most of the rocks in this area make it extremely difficult to determine if the fault continues bedding-parallel to the south, dies out, or is replaced by an unconformity tectonically flattened beyond recognition. We prefer the first alternative and have placed unit 2 into the younger section and units 4 and 5 in the older section. To the east, the contact between the intermediate and older

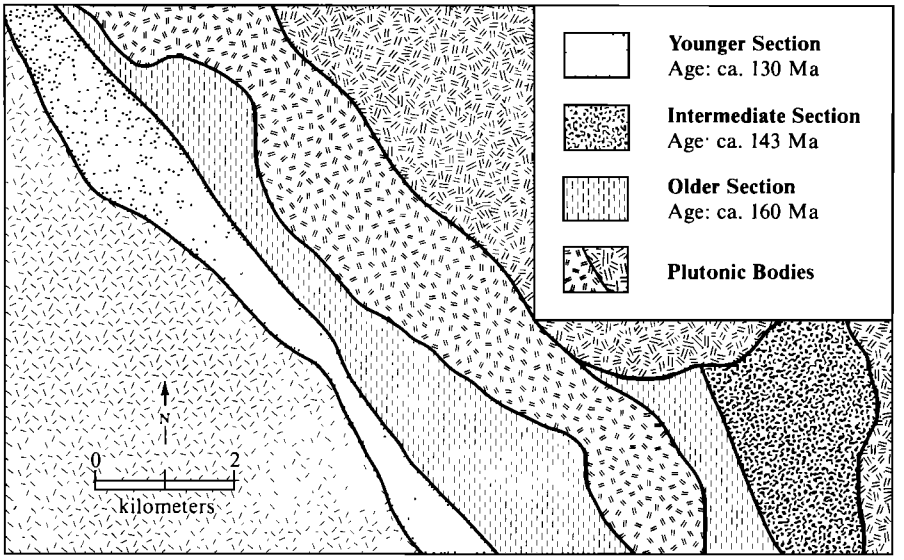

Fig. 2. Simplified diagram of Plate 1 showing the interpretation of the three main stratigraphic sections deduced from field and laboratory data. Pattern shown in southwest corner of diagram represents granitoid rocks of probable Cretaceous/Jurassic age (unit 13, Plate 1).

sections is also a fault, and is locally characterized by disruption in bedding orientation, changes in lithology, depositional environment, and strain characteristics, as well as considerable topographic expression. Since the older (160 MA) section lies to the west of the intermediate (143 Ma) section, and both sections dip to the west, there has clearly been fault repetition. We will suggest a model for generating this geometry in a later section.

Geochronology

Fossils have yet to be found in the Mt. Goddard section, but Pb/U zircon ages have been determined for several key volcanic and plutonic units. The isotopic data along with information on analytical procedures and uncertainties are given in Table 1. The locations of the geochronological samples are shown in Plate 1, and details on sample setting, zircon yield and preferred igneous ages are given in Table 2. The discussion below focuses on the interpretation of the isotopic data.

Igneous ages derived from the isotopic data fall in the 160 to 130 Ma range. Confident igneous age assignments are often based on the condordance or equivalence of the Pb-U and Pb-Pb ages in a given analysis (internal concordance). Such concordance is arrived at statistically by the overlap of the analytical uncertainties of the indigenous ages. On the 206Pb/238U:207Pb/235U concordia diagram [Wetherill, 1956], such overlap is exhibited by the error polygon of a given analysis intersecting the concordia line. A major problem in the interpretation of the Mt. Goddard data, and all mid-Paleozoic and younger zircon data sets, is the near linearity of lower concordia. Such linearity could permit the disturbance of the zircon isotopic system to be topologically expressed by downward migration of the error polygon without resolvable divergence from the concordia line. For this reason internal concordance alone has been referred to as apparent concordance [Saleeby, 1982]. The agreement of internally concordant ages from multiple fractions of a given zircon population split into different physical groups, or multiple samples from a given map unit is referred to as external or true concordance. The rationale here is that the effects of known multistage behavior are observed to vary with the physical properties of zircon grains, and are also observed to be heterogeneous over map-scale units (Silver [1964], Saleeby and Sharp [1980], as examples). Thus one should expect external concordance as a mark of single-stage behavior.

Examples of true concordance in the Mt. Goddard data set are exhibited in samples

TABLE 1. Mount Goddard Zircon Isotopic Age Data

Sample Number	Fraction Properties[1]	mg Analyzed	^{238}U ppm	^{206}Pb ppm r.g.	Measured Ratios		Radiogenic Ratios			Isotopic Ages (Ma)[2]		
					$\frac{^{206}Pb}{^{204}Pb}$	$\frac{^{206}Pb}{^{207}Pb}$	$\frac{^{206}Pb}{^{238}U}$	$\frac{^{207}Pb}{^{235}U}$	$\frac{^{207}Pb}{^{206}Pb}$	$\frac{^{206}Pb}{^{238}U}$	$\frac{^{207}Pb}{^{235}U}$	$\frac{^{207}Pb}{^{206}Pb}$
1	10/20											
	<45μ	2.2	220	4.1	206	8.23	0.02149	0.1476	0.04984	137.1	139.8	188±20
	45-80μ	1.9	190	3.6	876	14.87	0.02189	0.1524	0.05050	139.6	144.0	218±10
	80-120μ	4.8	148	2.9	136	6.28	0.02278	0.1613	0.05138	145.2	151.8	258±25
2	10/20											
	<80μ	13.8	289	5.3	302	10.24	0.02127	0.1445	0.04894	135.7	136.1	145±20
	80-120μ	20.8	292	5.4	182	7.71	0.02127	0.1431	0.04882	135.7	135.8	139±20
3	10/20											
	<80μ	16.6	876	18.9	1748	17.35	0.02489	0.1689	0.04924	158.5	158.5	159±10
	80-120μ	10.2	782	17.0	2365	17.98	0.02506	0.1707	0.04941	159.6	160.0	167±10
4	10/20											
	<80μ	11.9	305	5.8	1282	16.59	0.02199	0.1479	0.04882	140.2	140.1	139±10
5	3/20											
	<80	7.1	258	4.9	969	15.61	0.02208	0.1487	0.04888	140.8	140.8	142±10
6	10/20											
	<45μ	6.4	225	4.4	1396	16.77	0.02256	0.1527	0.04911	143.8	144.2	153±10
	<45μc	7.0	226	4.5	913	14.95	0.02289	0.1604	0.05084	145.9	151.0	233±10
	45-80μc	2.6	211	5.0	3485	15.42	0.02711	0.2259	0.06048	172.4	206.8	620±15
7	5/20											
	<45μ	9.4	396	8.9	2140	17.85	0.02445	0.1657	0.04916	155.8	155.7	155±10
	45-80μ	9.0	304	6.5	1509	16.86	0.02485	0.1698	0.04960	158.3	159.2	176±10
	80-120μ	15.1	171	3.7	1010	15.44	0.02522	0.1743	0.05027	160.6	163.1	208±10

1. Fractions separated by grain size and magnetic properties. Magnetic properties given as non-magnetic split at side/front slopes for 1.7 amps on Franz Isodynamic Separator. Samples hand-picked to 99.9% purity prior to dissolution; c = population dominated by colored or cored grains. Dissolution and chemical extraction techniques modified from Krogh [1973].
2. Decay constants used in age calculation: $\lambda^{238}U = 1.55125 \times 10^{-10}$, $\lambda^{235}U = 9.8485 \times 10^{-10}$ [Jaffey et al., 1971]; $^{238}U/^{235}U$ atom = 137.8 [Chen and Wasserburg, 1981]. Common Pb compositions used for non-radiogenic correction based on blank determinations and approximated from feldspar determinations on nearby Mesozoic granitoids [Chen and Moore, 1982; J.H. Chen, personal communication, 1983] Blank Pb: $^{206}Pb/^{204}Pb = 18.8$, $^{207}Pb/^{204}Pb = 15.6$; Initial Pb: $^{206}Pb/^{204}Pb = 19.0$, $^{207}Pb/^{204}Pb = 15.75$. Long-term reproducibility used in age uncertainties which slightly exceed combined effects of uncertainty in mass fractionation, spike uncertainty, counting statistics and uncertain initial Pb compositions (except where $^{206}Pb/^{204}Pb \ll 1000$). Analyses conducted at CIT between 1981 and 1984 during which total blank ranged from 1 ng to 50 pg, respectively. Uncertainty in $^{206}Pb/^{238}U$ ages ≈ 1%, $^{207}Pb/^{235}U$ = 1.5-2.0%. Mass spectrometer performance monitored on a regular basis by runs of NBS SRM 981, 982, 983 and U500 standards.

TARLE 2. Data on Zircon Sample Location, Petrography, Yield and Igneous Age Interpretation

Sample Number	Field Location	Field Setting	Petrography	Yield: ~mg Zircon/kg Sample	Notes on Interpretation of Isotopic Data	Preferred Igneous Age
1	Blackcap Mtn. 15' quad. 37°7.0'N. 118°45.4'W.	Felsic ash-flow tuff interbedded with volcaniclastic rocks	Plagioclase phenocrysts in a finely granular matrix of quartz and feldspar	20/86	Linear array of discordant points dispersed up from concordia lower intercept (Figure 2) defines inheritance or entrainment trajectory	131±6 Ma
2	Mt. Goddard 15' quad. 37°6.1'N. 118°44.2'W.	As above	Phenocrysts of plagioclase set in semi-equigranular mosaic of quartz, feldspar, and biotite	35/101	Single-stage system based on external concordance of multiple fractions	136±2 Ma
3	Mt. Goddard 15' quad. 37°7.1'N. 118°44.2'W.	100m thick rhyolite lava flow within interbedded mafic to felsic lavas and tuffs	Sparse phenocrysts of plagioclase in a finely granular mixture of quartz, felspar, and biotite; relic flow banding	40/60	As above	159±2 Ma
4	Mt. Goddard 15' quad. 37°4.6'N. 118°39.1'W.	Deformed felsic sill within volcanic section	Sparse plagioclase phenocrysts set in a fine-grained matrix of quartz and feldspar	12/107	Single-stage system based on external concordance with sample 5	140±1 Ma
5	Mt. Goddard 15' quad. 37°4.6'N. 118°39.1'W.	Deformed, locally brecciated, felsic sill within volcanic section	As above	8/102	Single-stage system based on external concordance with sample 4	140±1 Ma
6	Mt. Goddard 15' quad. 37°4.7'N. 118°38.8'W.	Felsic ash flow tuff interlayered discontinuously with volcaniclastic rocks	Phenocrysts of plagioclase set in fine-grained matrix which include lithic lapilli	20/105	Linear array of discordant points dispersed up from concorida lower intercept (Figure 2) defines inheritance or entrainment trajectory	143±3 Ma
7	Mt. Goddard 15' quad. 37°7.9'N. 118°44.4'W.	Deformed 1km thick sill-like mass within Mt. Goddard metavolcanic pendant	Fine grained granodiorite. Zircon population obtained from J.H. Chen; Chen and Moore, 1982-sample 75.		As above	156±2 Ma

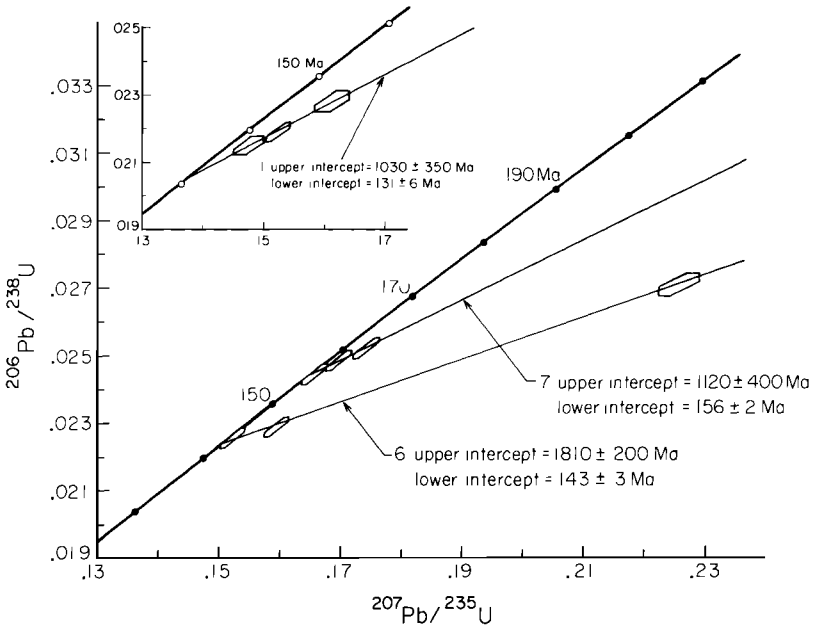

Fig. 3. Concordia diagrams for discordant samples from the Mt. Goddard section [after Wetherill, 1956]. Numbers indicate samples as shown on Table 1. Concordia intercepts for samples 1, 6 and 7 after York [1966]. Igneous age interpretations are given in Table 2.

2,3,4, and 5. The 206Pb/238U ages of each analysis carry the greatest precision, and thus these ages are used in the assignments of the preferred igneous ages in Table 2 (see also Plate 1). Internal and external discordances are observed in samples 1, 6 and 7. In each case discordancy is observed to be a function of increasing grain size and decreasing U concentration. On 206Pb/238U:207Pb/235U concordia diagrams (Figure 3) each of the discordant arrays disperse up from concordia lower intercepts. As can be seen from Figure 3 and Table 1, the lower intercepts of samples 6 and 7 correspond to internally concordant data points. The discordia arrays of samples 1, 6 and 7 and the relationships between discordance, grain size and U concentration strongly suggest the incorporation of older zircon into magmas that were erupted or crystallized at the approximate time of the lower intercept ages. These are shown as preferred igneous ages in Table 2.

Rocks of the Mt. Goddard pendant have undergone regional thermal metamorphism and thus the possibility of Pb loss should be considered. In terms of the discordant samples (1,6 and 7) the patterns observed are unlikely to be related to Pb loss. Greater discordance with increasing U concentration and decreasing grain size would be expected, along with downward dispersion of the discordia arrays from concordia upper intercepts [Silver, 1964; Saleeby and Sharp, 1980]. As discussed above this is the opposite of what is observed. Possible superpositioning of significant Pb loss over earlier two-stage systems is considered unimportant due to the linearity of the observed arrays, and the internal concordancy of the lower data points of samples 6 and 7. External concordancy of samples 2,3, 4 and 5 argue strongly for single-stage behavior for these systems and thus minimal Pb loss. On the whole the Mt. Goddard sample suite bears low U concentrations (150 to 400 ppm except for sample 3), which is consistent with the lack of any evidence for significant Pb loss.

Incorporation of ancient zircon by inheritance from the magma source regime or entrainment from wall rocks during magma ascent is exhibited quite clearly in sample 6. This sample was hand and sieve split into a clear fraction (<45μ) and two colored fractions (<45μ and 45-80μ). The coarser fraction contains faint cores. The fine clear fraction yields age data which are internally concordant. The fine colored fraction is discordant, and the coarse fraction is highly discordant with an age divergence of over 400 Ma. Coarse fractions

from samples 1 and 7 likewise contain rounded cores in some grains and yield the oldest most discordant ages, consistent with inheritance or entrainment. Zircon age data for a single analysis of an <80μ size fraction from sample 7 were reported in Chen and Moore [1982]. The reported ages were t 206Pb/238U = 157.0 Ma, t 207Pb/235U = 158.8 Ma, and t 207Pb/206Pb = 196 Ma. Such internal discordance led these workers to an ambiguous interpretation for the igneous age. Examination of the new data on three fractions split from the original population (Table 1) shows upward and downward dispersion of U-Pb ages and Pb-Pb ages from the ages reported by Chen and Moore [1982]. Such dispersion is the mark of a two-stage mixing array that was homogenized in the original single fraction analysis. Upper intercept ages are given for the discordant samples in Figure 3. Note the large uncertainties, which are a result of the clustering of data points near the lower intercepts. The upper intercept ages are not given specific significance in that they probably represent the overall isotopic character of the contaminate zircon which may itself represent a multistage system.

It is significant that each of the upper intercepts is well back into the Proterozoic, like numerous upper intercept ages determined for other Mesozoic metavolcanic and granitoid complexes of the Sierra Nevada [Saleeby et al., 1985; Sams, 1985; J.B. Saleeby, unpublished data, 1985]. Furthermore, DePaolo [1981] has resolved a major Proterozoic sialic component within Mesozoic granitoids of the Sierra Nevada by Nd and Sr isotopic studies. The wide array of upper intercepts given in the Figure 3 concordia diagrams is not surprising. Zircon studies in high-grade para- and orthogneisses of the southernmost Sierra Nevada, which are the only direct samples available for deep crustal materials beneath the range, show significant isotopic variability in Proterozoic zircon populations with the oldest components lying in the 1.8 to 2.0 Ga range [Sams, 1985]. Thus the ~1.8 Ga upper intercept of sample 6 may likewise approximate an upper endmember component in ancient crustal materials beneath the Mt. Goddard volcanic edifice.

The first-order implications of the zircon data reported here are that metavolcanic and shallow-level plutonic rocks of the study area fall between 160 and 130 Ma in age. The map distribution of these ages (Plate 1) along with the structural and stratigraphic data discussed previously indicate that the west-facing homoclinal sequence contains at least one structural repetition in the age (stratigraphic) sequence by faulting.

Metamorphic Grade

The volcanic section and the older plutons have undergone regional metamorphism related to widespread penetrative deformation, while contact metamorphism has affected rocks near larger plutons. Typical regional metamorphic mineral assemblages include:

mafic rocks: plagioclase + biotite + chlorite + actinolite ± (clinozoisite)

felsic rocks: plagioclase + quartz + white mica + epidote ± (chlorite + magnetite + hematite)

calcareous tuff: quartz + white mica + calcite + epidote ± (tremolite)

In addition, rare pelitic rocks bear almandine garnet, and the amphibole in mafic rocks, characterized by low z^c angles, is probably actinolite. Zones of piemontite-bearing schist occur locally. Anorthite content of plagioclase determined by universal stage measurements varies between An18 and An31 in mafic rocks, whereas in felsic rocks it varies from An14 to An24, averaging An16 (7 samples). The lower anorthite content in the felsic rocks may be due to a calcium-poor rock, but the apparent stable occurrence of the mineral pair plagioclase-epidote in many samples suggests this is probably not the case. According to Turner [1981] the anorthite content of plagioclase in amphibolite facies is >An20. The lower value in the felsic rocks along with the presence of actinolitic amphibole and piemontite, therefore, suggest that PT conditions may be slightly below those of the lower amphibolite facies.

Contact metamorphism of volcaniclastic rocks is often difficult to identify in the field except in mica-rich assemblages. Our observations indicate that contact zones are probably relatively narrow, and where present, rocks of suitable composition bear andalusite (sometimes the Mn-rich variety, viridine) and oligoclase (An18), placing these contact zones in the hornblende hornfels facies [Turner, 1981].

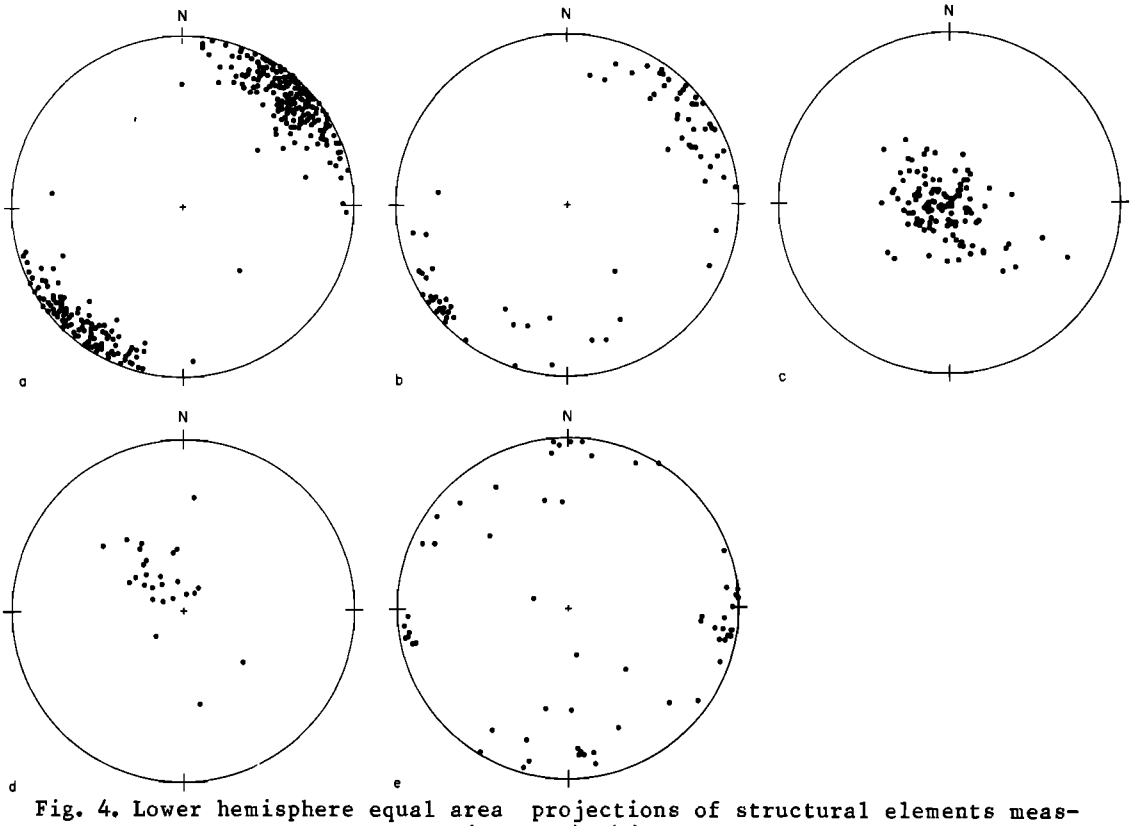

Fig. 4. Lower hemisphere equal area projections of structural elements measured from the Mt. Goddard area (Plate 1). (a) Poles to slaty-type cleavage; (b) poles to bedding; (c) lineations formed by elongate minerals and long axes of stretched lapilli (stretching lineation); (d) lineations formed by the intersection of bedding and slaty-type cleavage; (e) poles to axial planes of group B folds and crenulations.

Although we have separated the metamorphism into regional and contact stages, it is possible that both stages may be related to the heat associated with generation and emplacement of the batholith. In this view, regional metamorphism of the country rocks occurred while they were being penetratively deformed, whereas hornfelsic textures indicate annealing at a late stage after deformation ceased, and where the rocks were in closest proximity to the heat source. This concept fits well with the extensional model advanced later in the paper.

STRUCTURAL CHARACTERISTICS

General

The Mt. Goddard pendant represents a steeply dipping "homoclinal" screen separating large plutonic masses of the composite Sierra Nevada batholith. Bedding dips are predominantly steeply to the west or nearly vertical (Figure 4b), and are parallel or subparallel to slaty cleavage. Most other tectonic structures also have steep orientations. Two groups of tectonic structures are present: (A) slaty cleavage, lineations (intersection and stretching types), less common minor folds showing axial plane slaty cleavage, and ductile faults, all related to widespread penetrative deformation; and (B) minor folds showing axial plane crenulation cleavage, lineations (mostly intersection type), kinks, crenulations and crenulation cleavage, and brittle faults, all related to domainal deformation. Group B structures in the Mt. Goddard area are interpreted to postdate group A structures.

Group A Structures

The dominant structure of this group is the penetrative slaty cleavage present in

a

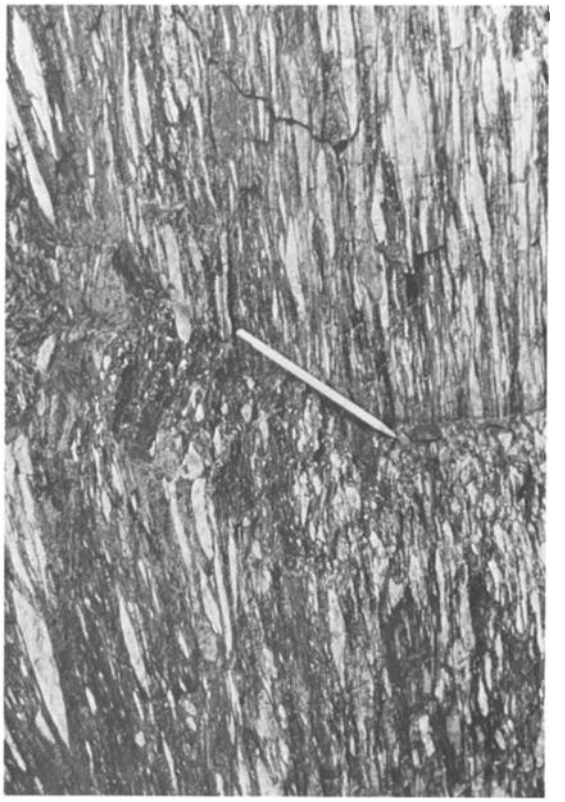

c

b

most exposures in the volcanic section. Its morphology ranges from nearly continuous [Powell, 1979] in fine tuffs to spaced disjunctive in massive rocks such as lava flows, and shows characteristics comparable to the cleavages developed in volcaniclastic rocks to the north [Tobisch, 1984]. The orientation of the cleavage is generally northwest in strike with a nearly vertical dip (Figure 4a).

Minor folds associated with the slaty cleavage are not common, but where present their axial planes parallel cleavage (Figure 5a), and their axes parallel bedding/-cleavage intersections. These lineations are moderately to steeply plunging (Figure 5b), generally in the northwestern quadrant (Figure 4d). Most minor folds show interlimb angles ranging from open to close (Figure 5a) and rarely tight [Fleuty, 1964]. Mappable folds are present in a few areas (e.g., northwest portion of Plate 1), but they do not repeat substantial portions of the stratigraphic section. Indeed, top directions are nearly all west facing, and the volcanic rocks essentially represent a composite west-dipping homoclinal section. Although bedding shows scattered orientations in some areas (Plate 1 and Figure 4b), these anomolies can be related to localized folding around steep axes or rotation near faults or large plutons.

A strong stretching lineation defined by aligned mica or other minerals, and by elongate volcanic fragments in the lapilli tuffs (Figure 5c) is probably the best-developed linear feature in the region. The stretching lineations plunge steeply (Figure 4c), and are often subparallel to bedding/cleavage lineations (cf. Figures 4c and 4d).

Because the volcanic section is lithologically monotonous and bears only occasional marker beds, documenting large-scale offset along faults formed during the ductile deformation is seldom possible. Two zones which most likely represent zones of ductile faulting occur in the northwest part of the area, and are represented by unit 3 (southern and northern sectors; Plate 1). The southern sector of unit 3 represents a fault zone spatially related to folds, the fault oriented essentially subparallel to the axial planes of the mapped folds (Plate 1) and the prevailing slaty-type cleavage. Blocky fracturing within parts of this zone are interpreted as evidence for renewed movement along this zone subsequent to cleavage formation. The northern sector of unit 3 (Plate 1) is characterized by an intensely laminated, platy phyllitic schist discussed earlier under the section on stratigraphy.

Group B Structures

These structures are distinctly domainal relative to those of group A. They have been observed mostly in units 1-6 (Plate 1), and only rarely in units 8-12. This is probably at least in part an expression of the higher strains and better cleavage development found in units 1-6 which provided a rock geometry more conducive to forming such structures. The dominant structures are represented by kinks, minor folds, crenulations, and locally crenulation cleavage. This folding of the earlier cleavage occurs around axial planes which have orientations here interpreted as two discrete sets: E-ESE and N-NNE (Figure 4e). Although the two data sets overlap (Figure 4e), field relationships suggest these sets have a conjugate relationship, and we base our interpretation on the observations that 1) neither set is seen to refold the other, 2) where both sets occur, they form conjugate crenulations or folds, and 3), the two sets are symmetrically disposed around the group A slaty-type cleavage (cf. Figures 4a and 4e). Conjugate folds with essentially the same orientation maxima have been reported from other parts of the Sierra Nevada [e.g., Ave Lallement et al.,

Fig. 5. Photographs of structural elements. (a) Group A fold, showing slaty cleavage paralleling its axial plane. Pencil is ca. 10 cm long; (b) group A bedding/slaty cleavage intersection plunges nearly vertically parallel to pencil (15 cm long), while group B crenulation axes (seen in slaty cleavage surface) plunge moderately to the left; (c) moderately stretched lapilli showing a constrictional symmetry (nearly plane strain; see sample W, Table 3) as seen on two orthogonal joint faces. Pencil is 15 cm long. Narrow shelf is a subhorizontal joint surface, whereas other joint surfaces dip very steeply. Note axial ratios of lapilli on subhorizontal joint surface are much less than those on steeply dipping faces.

1977; Bhattacharyya and Paterson, 1985], and there is no doubt they represent a regional phenomenon at least along the eastern Sierra Nevada continental arc. The above observations and data indicate that the conjugate set is geometrically related to group A slaty-type cleavage and may also be genetically related to it and/or to zones of ductile faulting as previously suggested for similar structures to the north [Tobisch and Fiske, 1976; 1982].

As with group A structures, lack of marker horizons renders it difficult to delineate faults associated with group B structures. Some group B faults have been mapped (Plate 1), and they also show a conjugate orientation symmetrically dispersed about the group A slaty-type cleavage. These faults were not observed to be associated with a crenulation or other type of cleavage.

Timing of Deformation

There is only sparse data presently available to help constrain the age of these structures. Since the three stratigraphic sections (160 Ma, 143 Ma, and 130-135 Ma) which comprise the volcanic section contain the same structural sequence, it is clear that the deformation postdates the youngest part of the section, which consists largely of felsic ash flow tuff (unit 1, Plate 1). The maximum age of the deformation therefore is ca. 131 ±6 Ma. The Lamarck and Mt. Givens plutons, which are tectonically undeformed and cut the volcanic section 3 km to the north [Bateman, 1965], yield radiometric dates of around 90 Ma [Stern et al., 1981]. Deformation then is presently constrained within the time period ~130-90 Ma.

Strains in the Volcanic Section

We analyzed rocks for strains at 29 stations in the field, mainly using lithic lapilli as strain markers (Figure 5c), but on occasion breccia fragments and vesicles in mafic lavas were used. The highly jointed rock provided ample opportunity to find exposures in which joints approximately paralleled two of the principal planes of the strain ellipsoid (X>Y>Z). Slaty-type cleavage was taken to approximate the (XY) plane, and other planes orthogonal to the cleavage and either normal (YZ) or parallel (XZ) to the stretching direction (X) approximated the other two principal planes. Strain markers were measured on two such joint surfaces at each station and the data processed according to the method of Elliott [1970] adapted for volcaniclastic rocks as outlined in detail elsewhere [Tobisch et al., 1977]. Results from each plane were then combined to obtain the strain magnitude ($\bar{\varepsilon}_s$) using the equation of Nadai [1963, p. 68]:

$$\bar{\varepsilon}_s = \frac{1}{\sqrt{3}}\left[(\bar{\varepsilon}_1-\bar{\varepsilon}_2)^2+(\bar{\varepsilon}_2-\bar{\varepsilon}_3)^2+(\bar{\varepsilon}_3-\bar{\varepsilon}_1)^2\right]^{\frac{1}{2}} \quad (1)$$

where $\bar{\varepsilon}_1>\bar{\varepsilon}_2>\bar{\varepsilon}_3$, $\bar{\varepsilon}=\ln(1+e)$, and $e=l-l_o/l_o$, where l=length after and l_o= length before strain. The symmetry of the strain (ν) was determined using Lode's equation [Lode, 1926, p. 932]:

$$\nu = \frac{2\bar{\varepsilon}_2-\bar{\varepsilon}_1-\bar{\varepsilon}_3}{\bar{\varepsilon}_1-\bar{\varepsilon}_3} \quad (2)$$

For reasons treated elsewhere [Tobisch et al., 1977], the calculated values represent at least a minimum strain, and are thought to approximate closely the whole rock strain in most specimens.

The location of individual samples is shown in Plate 1, the calculated data listed in Table 3, and the values of $\bar{\varepsilon}_s$ and (ν) plotted on a Hsu diagram (Figure 6a). As one can see by comparing these data, the magnitude and symmetry of the strain vary considerably, which is at least in part a function of the rock type.

From these data, we conclude the following regarding the magnitude and symmetry of the strains as well as the amount of thinning that the volcanic section has undergone:

1. The intermediate stratigraphic section (units 9-12, Plate 1, Figures 2 and 6b) shows a substantially lower strain magnitude (mean extension in X= +47%, contraction in Z= -36%) than the younger (X= +170%, Z= -63%) or older sections (X= +121%, Z= -54%; see also Figures 6d-6e). We interpret the lower strains in the intermediate section to reflect the generally massive, poorly bedded nature of the rocks in that area, as well as the abundance of dikes and sills which are more likely to resist internal deformation than the finer-grained volcaniclastic and ash flow units common to the younger and older sections.

2. The greater extension in the younger and older sections is also reflected in the larger component of constrictional symmetry characteristically shown in those

TABLE 3. Strain Data

Sample Number	ε_{XY}	ε_{YZ}	ε_{XZ}	$\bar{\varepsilon}_s$	ν	X	Y	Z
			Mt. Goddard Area*					
A	-	0.53	0.62	0.95	0.72	+ 67	+33	-53
B	-	0.43	0.57	0.84	0.50	+ 64	+22	-48
C	0.88	-	1.11	1.7	-0.59	285	-33	-61
D	-	0.72	0.93	1.4	0.54	120	39	-67
E	0.38	0.35	-	1.0	-0.05	108	- 2	-51
F	0.38	0.32	-	1.0	-0.09	115	- 7	-50
G	-	0.41	0.93	1.3	-0.12	156	- 5	-59
H	-	0.88	1.14	1.7	0.54	160	49	-74
I	-	0.32	0.80	1.1	-0.20	126	- 9	-52
J	-	0.56	1.25	1.8	-0.11	265	- 8	-71
K	-	0.36	0.42	0.64	0.71	41	21	-40
L	0.49	0.42	-	1.3	-0.08	151	- 3	-60
M	0.59	0.44	-	1.5	-0.15	198	- 8	-63
N	0.69	0.49	-	1.7	-0.17	245	-10	-68
O	0.50	0.46	-	1.4	-0.01	165	- 1	-61
P	-	0.45	0.70	1.0	0.29	92	13	-53
Q	-	0.25	0.49	0.69	0.03	65	2	-39
R	-	0.49	0.73	1.1	0.35	98	19	-56
S	-	0.62	0.92	1.3	0.34	123	21	-62
T	-	0.44	0.60	0.88	0.49	69	21	-50
U	-	0.26	0.44	0.62	0.19	53	5	-37
V	-	0.21	0.32	0.52	0.31	40	7	-32
W	-	0.21	0.45	0.64	-0.07	61	- 3	-35
X	-	0.33	0.43	0.64	0.54	42	16	-39
Y	-	0.25	0.35	0.51	0.43	39	12	-32
Z	-	0.29	0.32	0.50	0.80	30	18	-32
AA	-	0.16	0.33	0.59	0.19	49	4	-33
BB	-	0.29	0.31	0.49	0.88	27	19	-32
CC	-	0.41	0.64	0.92	0.29	81	12	-50
			Mt. Ritter Area†					
1	-	0.29	0.80	1.14	-0.25	130	-10	-52
2	-	0.81	1.05	1.56	0.54	128	40	-68
3	-	0.50	0.62	0.93	0.61	69	28	-52
4	-	0.40	0.45	0.70	0.78	42	27	-43
5	-	0.36	0.42	0.64	0.71	40	22	-40
6	0.25	0.70	0.84	1.39	0.47	123	35	-67
7	-	1.02	1.32	1.96	0.54	192	58	-77

ε_{XY}, ε_{YZ}, ε_{XZ} are the strains measured on those planes, $\bar{\varepsilon}_s$ is the strain magnitude [cf. Tobisch et al., 1977], ν is the strain symmetry, and values of X, Y, and Z are percent elongations or contractions parallel to the principal axes of the strain ellipsoid where X>Y>Z (see text).

*For localities, see Plate 1.

†For localities, see Figure 7, western part of area 3. Samples shown as dots, numbered 1-7 from south to north.

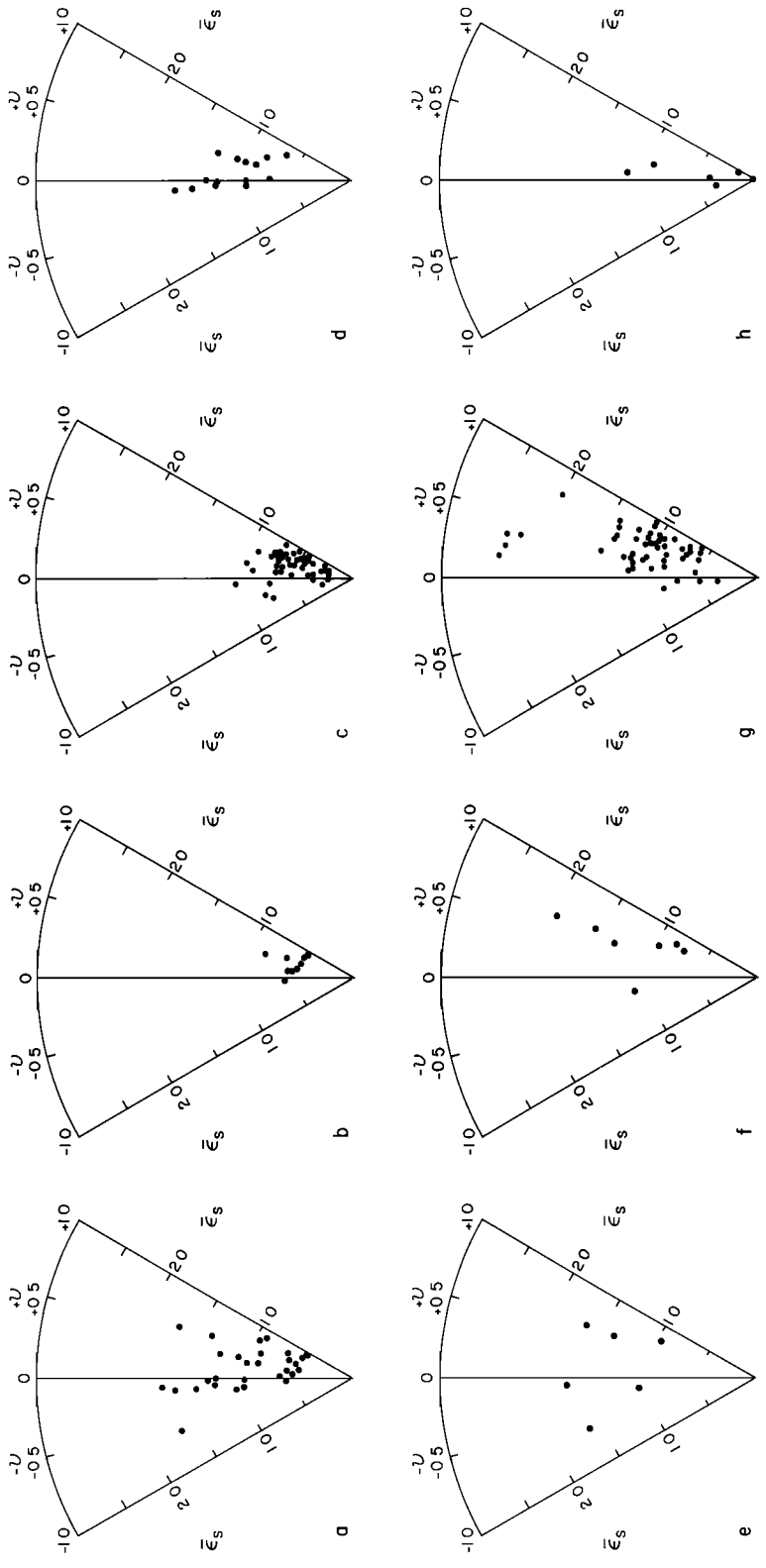

Fig. 6. Hsu diagrams [Nadai, 1963; Hsu, 1966] showing plots of strains from various parts of the sections: (a) Goddard area, all samples; (b) Goddard area, 143 Ma section, eastern part of region 3, Figure 7 (units 9–12, Plate 1); (c) Ritter area, 150–160 Ma section, region 2, Figure 7; (d) Goddard area, 160 Ma section, region 2, Figure 7; (e) Goddard area, 130–135 Ma section, western part of region 3, Figure 7 (units 1–2, Plate 1); (f) Ritter area, upper Jurassic–lower Cretaceous section, region 3, Figure 7; (g) Ritter area, upper Triassic–lower Jurassic section, region 1, Figure 7; (h) Ritter area, mid-Cretaceous section, region 4, Figure 7.

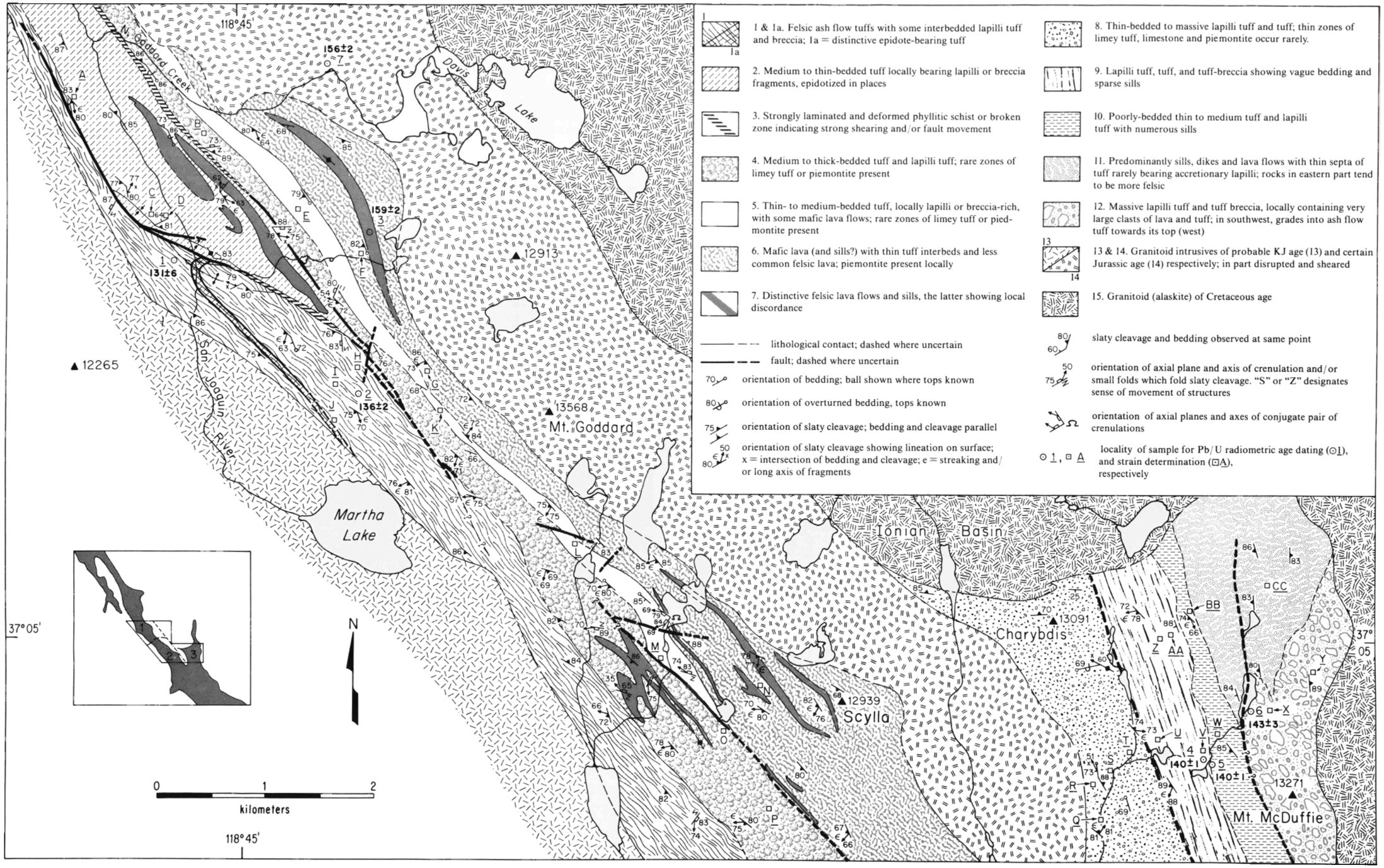

Plate 1. Geologic map of part of the Goddard area, modified after the maps of Bateman [1965] and Bateman and Moore [1965]. Contributions to the modification are shown in insert, lower left. Area 1: R. Fiske and O. Tobisch; area 2: J. Collander, S. Davis, J. Frey, and O. Tobisch; area 3: R. Fiske, J. Saleeby, and O. Tobisch.

rocks (Plate 1 and Table 3). Hsu plots from the older section (Figure 6d) show a clear tendency towards a plane strain (ν=0), one of the deformation paths previously suggested as characteristic of orogenic belts in general [Wood, 1973, Figure 10; Tobisch et al., 1977, p.35-36].

3. The steeply plunging bedding/slaty cleavage intersections (average ca. 70 degrees; cf. Figure 4d) associated with group A structures suggest that bedding may have been already steeply inclined prior to formation of the slaty-type cleavage. Using the method of Ramsay [1967, p. 129-132] for determining angular changes during deformation if the mean strain ellipsoid is known, we confirmed that the beds underwent only a small change in orientation during the cleavage forming process. Such a situation has also been documented in comparable rocks to the north in the Ritter Range [Tobisch et al., 1977, p. 36]. If one disregards the scatter of bedding due to localized deformation, the mean orientations of bedding and cleavage are nearly parallel (cf. Figures 4a and 4b). Given this and another generalization that the direction of maximum contraction is normal to the slaty cleavage, we can gain a rough estimate of the amount the stratigraphic section has been thinned. We have taken a WSW section in the southern part of the area (Plate 1) which passes roughly through Scylla and just south of Charybdis. The total thickness of the three stratigraphic sections (excluding the sill-like pluton (unit 14) in the older section) is approximately 6 km when measured normal to strike and the dips are compensated for. By using the mean values of contraction for each of the three stratigraphic portions given above, the presently observed thickness of 6 km had a precleavage thickness of approximately 12 km. This value of original thickness is a minimum, since it does not include thinning of the section by faulting which has undoubtably taken place in this area, but which is impossible to calculate because no suitable marker horizons exist.

COMPARISON WITH AREAS TO THE NORTH

General

Rocks in the Mt Goddard area are similar in many respects to those in the Ritter Range 85 km to the north (Figure 7). Both composite sections consist dominantly of pyroclastic rocks with a minor percentage of lava flows; chemically, both are dominated by rhyolite and basalt and only minor andesite; the depositional environment in both areas appears to have ranged from shallow marine to low-lying land, and both composite sections of rocks share many of the same structural elements in both character and orientation. A much greater range in protolith age is preserved in the Ritter area, however, with regions 1 (upper Triassic/lower Jurassic) and 4 (mid-Cretaceous) not represented in the Goddard area. Both the Ritter and Goddard pendants are composite west-dipping homoclinal sequences which show fault repetition of homoclinal sections of comparable age range (Figure 8). Faults which repeat the Ritter sections are, for the most part, intruded by sills which dip steeply eastward. The fault which repeats part of the Goddard section (described earlier in the section on Stratigraphy), however, is not intruded by sills. The structural succession in the two areas at least superficially appears the same (i.e., slaty cleavage followed by crenulations, etc.). Upon comparing the cross sections of Figure 8a and 8b, one is struck by the possibility that the Goddard screen is an isolated fragment of the intermediate interval (structural and stratigraphic) of the Ritter complex, or its lateral equivalent.

Strains

The strains shown in rock units of comparable age in the Ritter and Goddard areas show only slight correlation of magnitude and symmetry. In the 160 Ma section (region 2, Figure 7), the strains in the Goddard area show a greater magnitude and more constrictional component of symmetry than those in the Ritter area (cf. Figs 6d and 6c, respectively). While constrictional fabrics are common within faults, this change cannot be attributed to faulting alone, because both Ritter and Goddard areas are highly faulted [cf. Tobisch et al., 1977]. Strains measured in the 130-135 Ma section in the Goddara area (units 1-2, Plate 1) show relatively high magnitudes and considerable scatter in symmetry (Figure 6e). Rocks further along strike in the Ritter area (region 3, Figure 7), now known to be of comparable age as units 1-2 in the Goddard area [T.W. Stern, written communication, 1974], show strains which are comparable in magnitude to those of Goddard, but the latter show greater spread in symmetry and a greater tendency towards constriction (cf. Figures 6e-6f). Given the

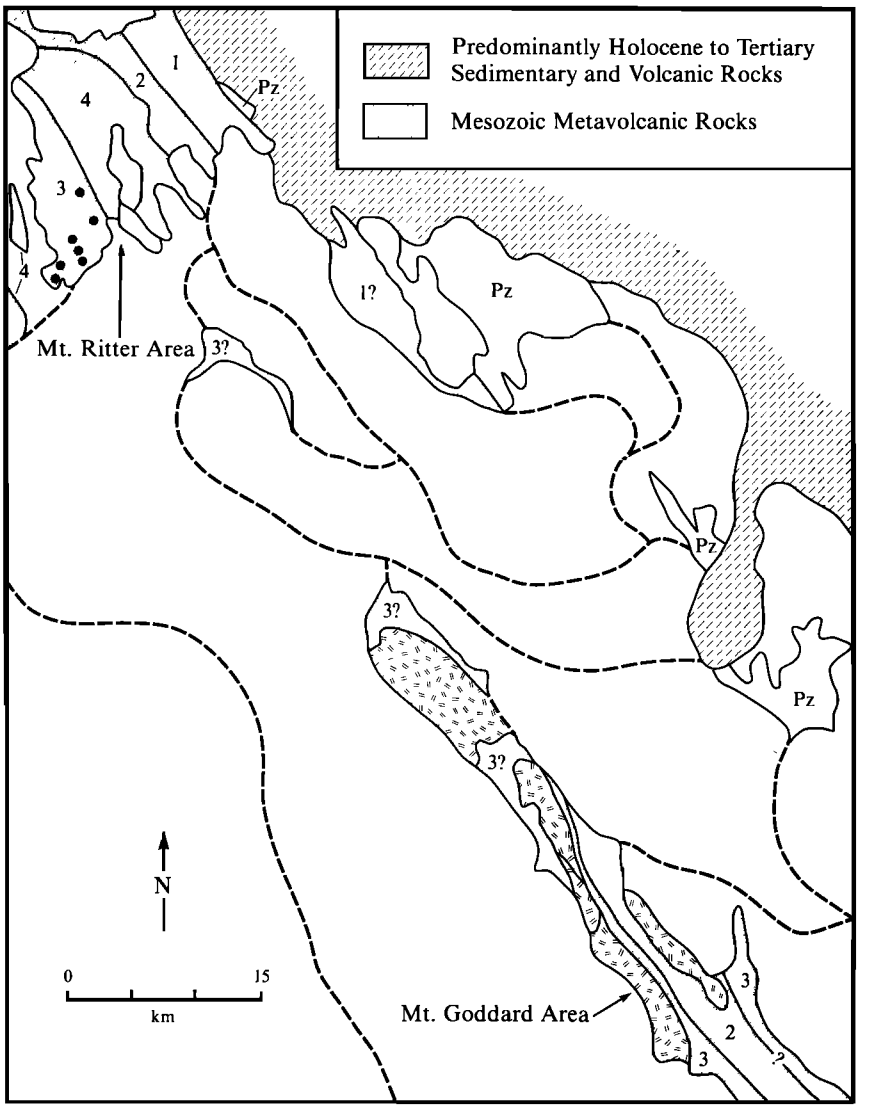

Fig. 7. Simplified map of the Goddard-Ritter area, showing main stratigraphic sections which are correlatable between the two areas. Age range of wall rock in the various regions is as follows: region 1: ~214-160 Ma; region 2: ~160-150 Ma; region 3: ~145-130 Ma; region 4: ~100 Ma; Pz: Paleozoic sedimentary rocks [Rinehart and Ross, 1964]. Source of radiometric ages given in Figure 8 caption. Areas showing igneous pattern indicate elongate (often deformed) plutons which are considered contemporaneous with the volcanic section (see text). Clear areas surrounded by dashed lines are approximate outlines of (for the most part) Late Mesozoic plutons showing strongly elongate forms oriented along NW strikes. Dots in region 3 of Ritter area indicate strain stations of samples 1-7, located sequentially from south (1) to north (7) (see Table 3). Figure is in part after Stern et al.[1981, Plate 1].

above and the data from upper Triassic/lower Jurassic and mid-Cretaceous sections in the Ritter area (Figures 6g and 7, region 1, and Figures 6h and 7, region 4, respectively), it is clear that considerable variations in strain magnitude and symmetry exist both parallel to and normal to the arc.

In summary, the strain data suggest that the Goddard area samples, while fewer in number than the Ritter suite, tend to show somewhat higher overall strain magnitude

and a greater component of constrictional symmetry (mean: $\bar{\varepsilon}_s$ =1.03; ν=0.22) than rocks in the Ritter area (mean: $\bar{\varepsilon}_s$=0.82; ν=0.71). The possible causes of such strain variation in these rocks are various, among them being (1) differences in physical conditions (P,T, etc.) of deformation, (2) differences in mechanical properties of the composite stratigraphic sections (3) fluctuation of overall stress magnitude, and (4) proximity of subvolcanic and/or older plutonic rocks acting as strain-resistent phacoids resulting in greater accumulation of strain in the volcanic section. Strong similarities of metamorphic mineral assemblages and lithologic suites from the two composite sections suggest that possibilities (1) and (2) are probably not fundamental causes of the mean strain differences shown. Possibilities (3) and (4), while more difficult to evaluate, are more likely important contributors, although a definitive model is not presently possible from the data available.

TECTONIC FRAMEWORK

General

We have considered the variation in Mesozoic volcanic stratigraphy, geochronology, and strains in one of the better studied portions of the arc in order to evaluate more rigorously the larger tectonic framework within which such structures are likely to evolve. The principal question that remains is, did the tilting of the beds and the generation of penetrative structures within the arc occur in response to (1) deformation related to accretionary collision processes within a compressional framework, (2) deformation related to magma emplacement within an extensional tectonic setting, or (3) some combination of both?

Compressional Model

To date, most workers have considered the structures in the Sierra Nevada to have been generated by regional compression [e.g., Bateman and Eaton, 1967; Moores, 1970; Schweickert and Cowan, 1975; Moores and Day, 1984; Schweickert et al., 1984b; Day et al., 1985]. In the accretionary collision model, the volcanic arc and related rocks of the western foothills are considered to have collided with the continental margin in the late Jurassic Nevadan orogeny. This compressional event is thought to have imposed the northwest oriented structures on rocks throughout the orogen. Bateman and Clark [1974] suggest the Nevadan orogeny occurred between approximately 140-150 MA, while Schweickert et al. [1984b] suggest an age of 155 ± 3 Ma. Both these estimates are based on data which comes largely from the Western Metamorphic Belt. Nokleberg and Kistler [1980] suggest a broader time span for Mesozoic deformation in the roof pendants not necessarily associated with the Nevadan orogeny, but they do not address the regional cause of the deformation.

The collisional model, however, does not account for the fact that parts of the pre-mid-Cretaceous volcanic section in both the Mt. Ritter and Mt. Goddard areas are younger than the proposed Nevadan orogeny, and that unconformities of Nevadan age have yet to be recognized in spite of detailed mapping in these areas. As there are no documented post-Nevadan collisional events in the Sierra Nevada, it is conceivable that Cretaceous collision events taking place in the Franciscan Complex to the west may have transmitted enough energy to the Sierran orogen to form the structures in question. Terrane accretion in the Franciscan of central California, however, can at most be correlated only with gentle folding and minor unconformities within the Great Valley sequence [Saleeby et al., 1985]. We conclude, therefore, that while there may be a case for major accretion in the Western Metamorphic Belt, it cannot be responsible for the structures we observe in continental arc rocks younger than Middle Jurassic in the eastern Sierra Nevada, at least in the 100 km segment under consideration.

Another major alternative under consideration, that of structures forming as part of the dynamic evolution of the subduction arc system itself, is more attractive but also presents a number of difficulties. One of the main problems is the question of whether or not the downgoing slab in a subduction zone will always transmit compressional strain to the arc lying in the upper plate some 200 or more kilometers away. It is well known from seismic data that subduction zones can vary considerably in dip, and some workers have classified the diversity into two general end members, gently dipping (Chilean or C-type) and steeply dipping (Marianas or M-type; Uyeda and Kanamori [1979]; Uyeda [1982]). C-type subduction zones are characterized by strong mechanical coupling between the subducting slab and the upper plate, and compressional structures develop in the

trench and forearc [Karig et al., 1979; Dewey, 1980]. M-type margins, on the other hand, show a weak mechanical coupling, and their forearcs are characterized by extensional structures [e.g., von Huene et al., 1980; Hussong and Uyeda, 1982]. M-type margins, therefore, are not likely to produce much contractional strain within the arc. While this two-fold classification does not consider likely complexities such as changes in the rate of plate advancement vs retreat of the subduction hinge (i.e., the process of "roll-back", Molnar and Atwater [1978]) as well as various other factors [Dewey, 1980], it will suffice for the present discussion.

If the subduction process is responsible for producing a compressional framework in the continental volcanic arc under consideration, a strong coupling between upper and lower plates would be necessary, implying a C-type. However, there is little evidence of significant compression having operated over the Great Valley forearc region. Thus, if this mechanism had in fact operated, the regional shortening strains would have been concentrated within the thermally softened arc, while the forearc remained rigid or became only weakly deformed. One would expect the subhorizontal compression to generate large-scale folds repeating substantial parts of the section, but such structures are not present in the 100 km segment of the arc being discussed. Furthermore, it is known that high-level extensional structures are a dominant feature along the magmatic axis in the type example of a C-type subduction arc system [Pitcher, 1978; Dalmayrac and Molnar, 1981]. In light of the above, we consider it unlikely that a model invoking regional compression is viable as a deformation mechanism to generate structures in the rocks in question. This brings us to consider the role of extensional tectonics and the dynamic evolution of the magmatic arc itself to explain the deformational patterns observed.

Extensional Model

General. As outlined recently [Tobisch et al., 1985], applying the concept of regional extension to explain the evolution of structures observed in the continental volcanic arc clarifies a number of hitherto puzzling features. Chief among these are the facts that (1) the volcanic sections in both the Mt. Ritter and Mt. Goddard areas are essentially composite homoclinal, and are almost devoid of tight to isoclinal folds of sufficient size that would be necessary to explain the steep dips and homoclinal nature of the beds; (2) the youngest parts of the homoclinal sections are strongly deformed but recently determined age data indicate they are post-Nevadan age; (3) we have not found unconformities in the pre-mid-Cretaceous section despite detailed mapping, suggesting that the regional deformation was not instigated until after the last beds were deposited, i.e., early Cretaceous; (4) strain evidence indicates that beds were at high tilts prior to the ductile deformation that formed the cleavage [Tobisch et al., 1977; this paper]; and (5) parts of the volcanic section are repeated by faulting resulting in the repetition of age sequences through the homoclinal sections.

These enigmas can be resolved if we consider a model which involved regional extension during Cretaceous time for the area of the Sierra Nevada presently underlain by the batholith. Although the detailed nature and exact extent of the extensional framework is still uncertain, we consider it likely that it is related to lithosphere-scale tumescence arising from subduction zone heating and magmatism. Batholith emplacement is considered an integral part of such tumescence, dynamically linked to, but not the sole cause of, regional extension and resulting structures.

We envision the deformation as occurring in two stages: (1) tilting of beds along listric normal faults during regional extension as magma and its thermal welt rise upward, and (2) subsequent imposition of tectonite fabrics on the tilted section during emplacement of the batholithic components. Although it is known that magmatic arcs can go through alternating phases of compression and tension [Dewey, 1980; Hussong and Uyeda, 1982], which might give rise to the structural sequence we have described, we envision the extensional framework as long lived (i.e., ca. 40 m.y.) and that both the tilting of the beds and the internal deformation seen in the volcanic sections are closely tied to the generation and emplacement of the batholith. Relating deformation in the Sierra Nevada wall rocks to some aspect of pluton emplacement is not necessarily new [e.g., Kistler et al., 1971; Bateman et al., 1983], and several workers have suggested general models which envision batholithic emplacement taking place in an extensional

environment with magma emplacement responsible for deformation of the wall rocks [Hamilton and Myers, 1967; Gastil, 1979; W. Hamilton, written communication, 1981]. These concepts have not been explored at specific sites, however, and they have remained controversial, since many workers considered the plutons to be predominantly passively emplaced with wall rock structures predating pluton emplacement [Kistler, 1966; Brook et al., 1974; Russell and Nokleberg, 1977; Nokleberg and Kistler, 1980].

Deformational Sequence Encapsulated. Figures 8a-8b show age relationships in different parts of the volcanic sections in the Mt. Ritter and Mt. Goddard areas, which we interpret as representing the two-fold sequence of events mentioned above. This sequence is conceptually illustrated in Figure 8c (i-iv). In the bed-tilting phase of the deformation, each fault block contains younger strata which overlie older rocks in the fault block below (e.g., in Figure 8c, ii, bed 2 in block II overlies bed 3 in block I). In addition, the bedding in the rotated blocks dips in the opposite direction from the dip of listric normal faults. This geometry has been documented in the Great Basin area by various workers [e.g., Proffett, 1977; Wernicke, 1981; Gans and Miller, 1983]. Subsequent ductile flattening, however, will substantially steepen the dips of both the beds and listric normal faults. Given the 50% flattening of the section documented earlier, a simple geometric reconstruction shows that beds with a tilt of (for example) 60° W and listric normal faults dipping 45° E will be rotated to dips of about 85° W and 75° E, respectively. In this situation, beds on both sides of the fault will dip steeply (and homoclinally) in one direction while the fault will dip steeply in the other (Figure 8c, iv). Since the strike of the bedding in the idealized case will parallel the strike of the listric normal fault, older parts of the section in one block will crop out on the "up-section" side of younger rocks in the contiguous block (e.g., in Figure 8c, iv, bed 4 in block II crops out "up-section" of bed 1 in block III), giving the appearance that older beds "overlie" younger beds along a fault. This geometry occurs where both bedding and listric normal faulting have been rotated to very steep but opposing dips. Where the rocks have been subsequently subjected to strong ductile flattening and metamorphism, the fault separating contiguous blocks can become cryptic. Our field data from the Mt. Goddard and Mt. Ritter areas are commensurate with such a model (cf. Figure 8a and 8b with Figure 8c, i-iv).

Deformational Stage 1. We consider the early deformational stages of the volcanic pile as being accompanied by rising of plutonic bodies encased in a thermal welt. Regional tumescence supplemented by that associated with the rising plutons reaches the base of the volcanic edifice, and the volcanic pile starts extending roughly parallel to bedding (Figures 8c, i, and 9a). As expansion continues, the developing listric normal faults will probably root into a décollement near the base of the volcanic edifice. The geometry of the listric normal faults allows these blocks to rotate to relatively steep dips of the bedding without the necessity of extreme extension in the crust (Figure 9b). The décollement is thought to roughly coincide with the upper surfaces of the thermal-plutonic welt. Unlike décollements in some metamorphic core complexes where the zone is lithologically controlled [e.g., Miller et al., 1983], the easterly dipping surface of the thermal-plutonic welt may cut obliquely through the volcanic section (Figure 9b), and horizons of different age may be exposed at the base of the blocks as they tilt. We suggest this is the case in the Mt. Ritter area, where the base of the juxtaposed units is successively older to the east (Figure 8a), supporting the interpretation that the décollement transgressed the bedding at deeper levels.

In the model introduced above the geometry and timing of initial deformation is related to the early members of the Cretaceous batholith which crop out as a belt along the western margin of the Sierra Nevada west of the tilted metavolcanic sections [Evernden and Kistler, 1970; Saleeby et al., 1985]. Crystallization ages on such plutons cluster in the 125 to 100 Ma range with a general eastward migration through time [Saleeby and Sharp, 1980; Stern et al., 1981; Chen and Moore, 1982]. Early members of the western Cretaceous batholith are predominantly gabbroic to dioritic in composition, and have been interpreted as constituting the roots of an andesitic volcanic chain [Saleeby and Sharp, 1980; B. W. Chappell and J. B. Saleeby, unpublished petrochemical data, 1981].

Figure 9a depicts the Goddard-Ritter sections as a thick pyroclastic sequence

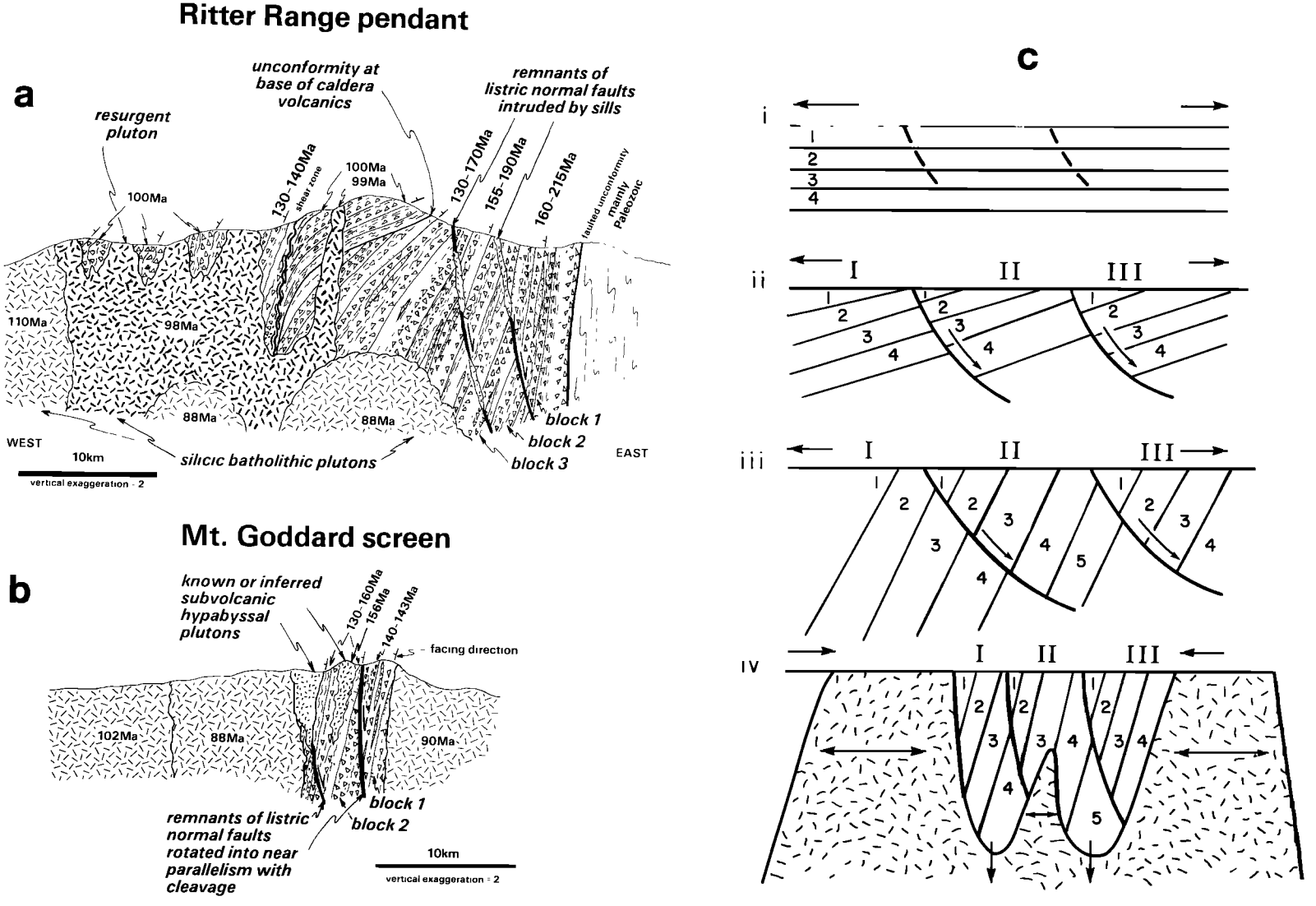

Fig. 8. Diagrammatic cross-sections of (a) the Ritter Range complex and (b) the Mt. Goddard screen. Explanations in text. Age data for the Ritter section are from Fiske et al.[1977], Fiske and Tobisch [1978], Stern et al. [1981], and T. W. Stern and J. B. Saleeby, unpublished data, 1975-1985). Age data for the Goddard section from this study and Stern et al. [1981]. (c) Diagrammatic illustration showing the proposed development of listric normal faults during extension followed by ductile flattening of the rocks related to intrusion of the batholith. See text for explanation.

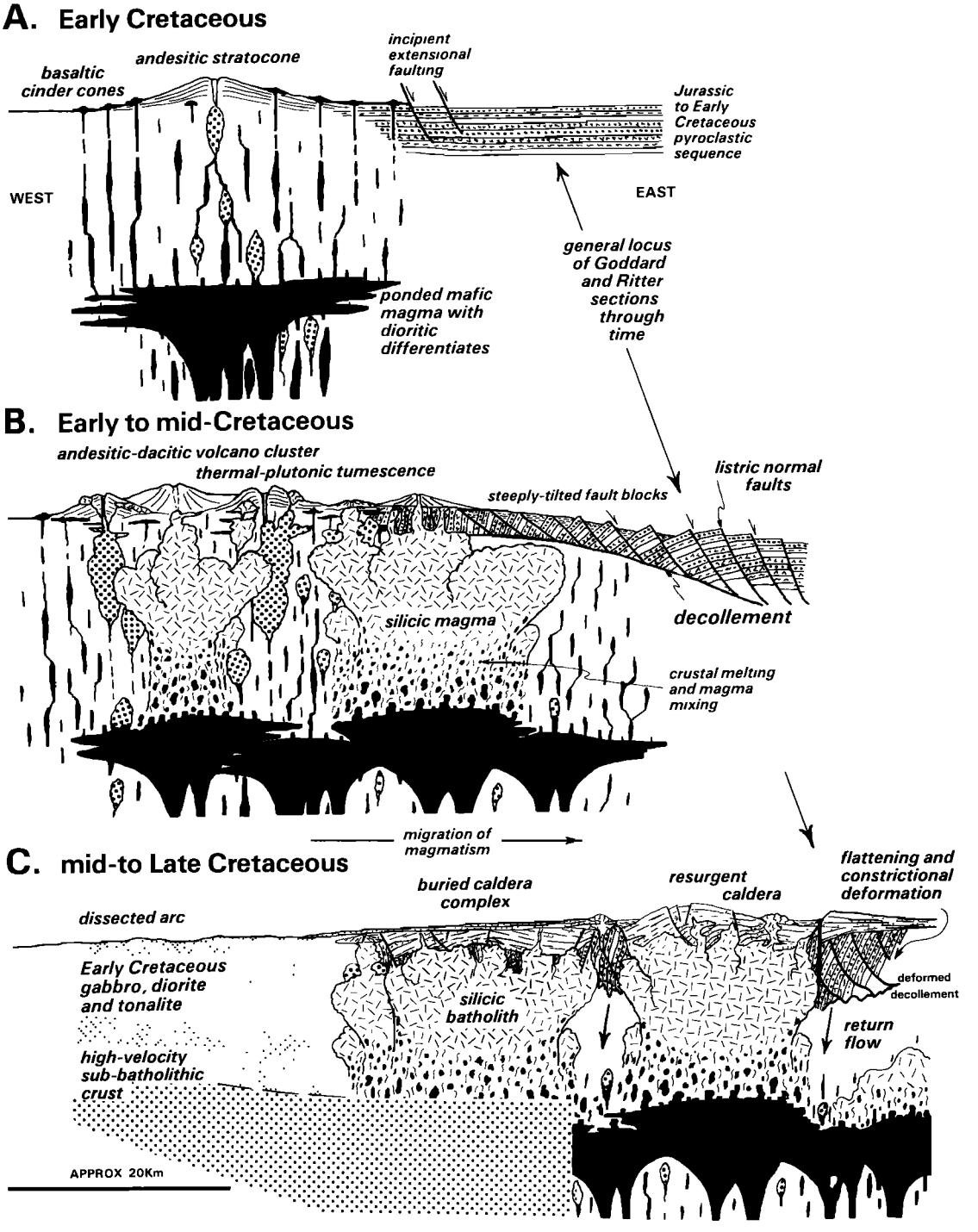

Fig. 9. Figure illustrating the regional framework within which the geometry and events shown in Figure 8 developed. See text for explanation. Evolution of volcanic and plutonic levels based on regional age patterns [Saleeby and Sharp, 1980]; Stern et al., 1981; Chen and Moore, 1982], and on models of caldera cycles [Fiske et al., 1977; Hildreth, 1981; Lipman, 1984]. Model of deep batholithic structure after Hildreth [1981], DePaolo [1981], and Saleeby et al. [1985]. Topographic relief of volcanic constructional and extensional faulting environment is exaggerated for clarity.

lying to the east of the early Cretaceous andesitic chain. This model is based on the succession observed in the modern Chilean Andes [Hildreth et al., 1982; W. Hildreth, personal communication, 1985] and on the time, compositional and spatial relations observed across the central Sierra Nevada batholith. The pyroclastic sequence shown includes rocks as old as early Mesozoic. Unconformities within the volcanic sequence related to Jurassic accretionary events have not been observed in this part of the arc, and the Jurassic to early Cretaceous sequence, which is considered to consist largely of distal deposits, is shown as a continuous, subhorizontal stratigraphic pile.

Subsequent magmatism in the western Cretaceous belt was dominated by voluminous silicic (dominantly tonalitic) plutons which appears to have migrated eastward from the andesitic (gabbro-diorite) chain. This model also predicts the presence of complex unconformities at the base of mid-Cretaceous silicic volcanic rocks, such as the Minarets Caldera in the Ritter Range [Fiske et al., 1977; Fiske and Tobisch, 1978]. Other possible remnants of such unconformities are presently under investigation in areas south of the Goddard pendant [Longiaru, 1985; J. G. Moore and J. B. Saleeby, unpublished data, 1984). In addition, the extensional environment depicted in Figure 9 is considered an integral part of the arc, and not necessarily related to back-arc spreading. The regional trend of extensional structures is considered to follow the NW-NNW trend of the early Cretaceous batholithic belt. Such a regional fabric in extensional structures and tilted sections may have provided preferred pathways for subsequent late Cretaceous plutons which show a pronounced NW elongation (Figure 7).

Deformational Stage 2. The next phase in the deformation history of the metavolcanic sections consisted of large silicic plutons elongated in a NW orientation (Figure 7) moving into upper crustal levels and intruding the steeply tilted section roughly parallel to bedding. Emplacement of successive pulses of magma into the volcanic section is thought to have occurred (at least initially) as sill- or possibly blade-like bodies [cf. Fiske and Jackson, 1972] that expanded as magma was added. It is envisioned that the sill-like bodies were expanding at a rate greater than could be accomodated by regional extension. Such a dynamic framework could produce substantial subhorizontal stress approximately normal to the tilted sections (Figure 8c, iv), imposing strong flattening ± constrictional fabrics on the wall rock. This ductile event was greatly facilitated by heat and fluids from the invading plutons. As a result, the thick volcanic sections were thinned overall by about 50% normal to bedding. In addition, we propose that deformation was enhanced by relative downward return flow of and stretching within the wall rock. Strongly developed, steeply plunging extension lineations (Figures 4c and 5c; Tobisch and Fiske [1982, Figure 5c]) and extensional fault movements related to cleavage formation (see map patterns in Tobisch et al., [1977, Figure 2a]) are interpreted as evidence for the downward extension and movement of the pendants relative to the rising plutons.

An additional structural consequence of this flattening of the stratigraphic sections was to essentially remove substantial parts of the overlying wall rock without recourse to massive stoping, and to rotate the listric normal faults to steep dips. Since our model appeals to batholith emplacement as a deformational agent, we envision the deformation as being diachronous, migrating eastward at about 2 to 3 mm/yr with the locus of mid- to Late Cretaceous arc magmatism [(Chen and Moore, 1982]. The entire crust is considered to have undergone considerable expansion with compensation of lower crustal volumes attained by influxes of mantle-derived mafic magma [DePaolo, 1981; Hildreth, 1981; Saleeby et al., 1985]. The magnitude of return flow within wallrocks bounding the rising plutons is dependent on the volume of crustal material melted and ultimately transported to high structural levels relative to the volume of mantle-derived material added to the lower crust and mixed with the silicic magmas. Fluid dynamic considerations suggest substantial return flow deformations within wall rocks up to about one magma body radius from the ascending pluton, and smaller increments up to within ten magma body radii [Grout, 1945; Marsh, 1982, 1984]. This raises the possibility that a significant component of strain observed in the Goddard and Ritter pendants may be related to return flow in addition to that imposed by horizontal compression related to magma chamber inflation. Repeated, episodic increments of these processes during successive stages of batholith development could explain the repeated parallel deformations previously

reported from the Ritter Range area [Tobisch and Fiske, 1982].

The presence of the 100 Ma Ritter Range (Minarets) caldera complex [Fiske et al., 1977] indicates that a sequence of ignimbrite activity, caldera resurgence, and deformation extended into Late Cretaceous time (Figures 8a and 9c). Of significance here is the strong domainal deformation observed in the 100 Ma Ritter caldera eruptive sequence [Tobisch and Fiske, 1982], and the tight age bracket of this deformation provided by cross-cutting relations of the resurgent intrusive sequences (Fig. 8a). Strong rotational deformation of caldera sequences during their magmatic and structural evolution is a well-documented phenomenon [Lipman, 1984], and the structural relations observed in the Ritter complex suggest that the caldera eruptives along the east side of the caldera were involved in deformation along with the older tilted sections.

CONCLUSIONS

From the data at our disposal, we conclude that generation of the majority of structures and variation in strains within the segment of the continental arc under considerations are more likely to be related to the internal dynamics of the arc itself, rather than to externally imposed tectonic events such as collision accretion. These dynamics involved the imposition of an extensional environment on the supracrustal volcanic section during massive batholithic emplacement throughout much of the Cretaceous. Extension occurred normal to the belt in a general NE-SW orientation which generated listric normal faults striking parallel to the orogen. As extension continued, bedding was rotated to steep dips along these faults, resulting in a series of steeply tilted, elongated fault blocks striking parallel to the belt, and which lacked large-scale folding of any areal importance. Subsequent rising of magma, often emplaced as elongate sill-like bodies, worked its way into the steeply tilted fault blocks approximately parallel to regional bedding, expanding at a greater rate than regional extension could accommodate. The overall dynamics of this magma tumescence imposed strong tectonite fabrics on the wall rocks, and reduced the volcanic section normal to bedding by about 50% overall. This process was facilitated by heat and fluids from the plutons and from downward return flow of the faulted stratigraphic sections relative to uprising plutons especially at middle and later stages of deformation, when the increasingly flattened keel-like geometry of the composite sections offered less resistance to sinking. Both rotation of beds and subsequent tectonite fabrics are post-Nevadan age and were imposed either continuously or episodically during Early to Late Cretaceous.

In this model, deformation of the wall rocks is considered to be related to batholithic emplacement. The deformation, therefore, is envisioned as being diachronous, advancing eastward at about 2 to 3 mm/yr with the locus of arc magmatism, but probably overlapping in time and space both parallel to and normal to the arc as successive families of plutons were emplaced. The relatively constant orientation of structures between pendants is probably a function of the constant orientation of the subduction zone which controlled the crustal tumescence (regional extension) and hence the orientation of tilted fault blocks and the subsequently emplaced plutons.

The structural and stratigraphic relations presented above for the Mt.Goddard and Ritter Range pendants, and the extensional model for generating the dominant structures in the continental volcanic arc carry important implications for the Nevadan orogeny. Various workers have suggested a Nevadan event involving collision of an oceanic arc with the continental margin for generating compressional structures in the western Sierra Nevada [e.g., Moores, 1970; Schweickert and Cowan, 1975; Moores and Day, 1984; Schweickert et al., 1984b; Day et al., 1985]. Since the continental volcanic rocks of the area under consideration in the eastern Sierra Nevada are predominantly distal deposits and were likely to have been nearly flat lying at the time of the proposed collision, large-scale folds (i.e., longitudinal strain) would no doubt have been generated from that event. Major folds of any areal importance, however, are largely absent in the area. Furthermore, stratigraphic breaks of Nevadan age have not been observed within the volcanic section in the Goddard or Ritter pendants. This raises several possibilities: (1) the volcanic arc in the Western Metamorphic Belt was emplaced into its present position by a mechanism other than collision such as transform related strike-slip movement common in some volcanic arc environments [Dewey, 1980]. In this view, Nevadan structures could be strongly developed in the

western Sierra Nevada while absent along the continental volcanic arc; (2) Nevadan structures north of latitude 37°30′ may be developed primarily within east-directed nappes of the western Sierra Nevada foothills as a result of a compressional event [Moores and Day, 1984; Day et al., 1985; Ricci et al., 1985; Saleeby et al., 1985], with the advancement of such nappes limited to the forearc region of the continental arc. It must be reemphasized, however, that silicic volcanism of the Goddard and Ritter pendants appears to have continued during the Nevadan event. This may be easier to explain with the strike-slip intra-arc transport of a Jurassic arc fragment from a different collision site into the Sierra region during continued subduction and related silicic volcanism of the continental arc.

A final point is that strain which produces tectonite fabrics in metamorphic rock is perhaps too readily interpreted as resulting from regional crustal shortening tectonics. In regions of voluminous magma emplacement, the dynamics of successively injected sill-like bodies, laterally spreading magma chambers and the return flow of less boyant wallrocks required by material balance during magma ascent should be evaluated very carefully before the associated metamorphic tectonites are simply considered products of regional crustal shortening. Indeed, voluminous magmatism should be considered a tectonic event of significant regional consequences.

APPENDIX: SOME UNCERTAINTIES OF THE MODEL

Listric Normal Faults

The number of these faults shown in Figure 9 is much greater than that actually identified in the field, and in fact their locality is often difficult to pin down with any precision. We have identified only one such fault in the Goddard area, while we think we can identify two and perhaps a third such fault in the Ritter area. The fault separating blocks in the Mt. Goddard area shows the most convincing field characteristics as described in the text, and it is relatively easy to identify. Those in the Ritter Range are more cryptic. Geologic evidence, however, indicates repetition of certain distinctive units while facing directions remain constant. In addition, sills which we consider to have intruded one of the faults dip eastward, while the volcanic section dips westward (cf. Figure 8a). Most compelling is the chronological evidence from fossil and Pb/U ages, which indicates that the faults must be present in the volcanic section even if their precise placement in the field is often difficult. It is not possible to document the original listric geometry of these faults because the substantial ductile flattening has rotated the faults to high dips.

We have collected an additional suite of specimens for Pb/U dating from the Ritter Range and are carrying out more detailed mapping in certain critical areas in an effort to pin down as precisely as possible the locality and geometry of the listric faulting we have proposed. A full report will be forthcoming.

Mechanism of Ductile Deformation

Our proposal suggests that pluton emplacement has imposed tectonite fabrics on the volcanic section. This is speculative, of course, and was born from the fact that no known regional post-Nevadan event exists in the eastern Sierra Nevada which can account for the late age of deformation in the continental volcanic arc except batholithic emplacement.

Much work needs to be done to confirm our proposed model, not only in documenting age relations between plutons and wall rock, but possibly more so in investigating the possible modes of emplacement of the plutons, and the effect intruding magma has on the wall rock. There is abundant literature from various orogens on diapiric emplacement and its late-stage effects on wall rock. From many reports in the Sierra Nevada, however, such emplacement is not thought to be widespread, leading to the notion that the plutons were largely passively emplaced. Our knowledge concerning other types of magma emplacement, such as inflation of sill-like bodies that might produce the elongate forms so commonly found in the central Sierra Nevada, and which we speculate may be a major contributor to the deformation of the wall rocks, has been relatively less well researched. This is an area for fertile investigation in field, theoretical, and experimental studies (cf. for example, Marsh [1982], Fiske and Jackson [1972]), and would contribute much to supporting or rendering invalid the mechanisms of deformation we propose.

Acknowledgements. Field and laboratory work has been supported in part by the U.S. Geological Survey, the Fluid Research Fund of the Smithsonian Institution, a Faculty Research Grant from the University of California, Santa Cruz, and N.S.F. grant EAR 8206478 awarded to Tobisch. Geochronological work was supported by N.S.F. grants EAR 8018811 and EAR 8218460 awarded to Saleeby. Patience and expertise in hand purification and sorting of zircon fractions by Cherilyn Saleeby was essential for this study. We are grateful to T. W. Stern of the U.S. Geological Survey for his important contributions in age dating of the Ritter Range rocks, the complete report of which will be published elsewhere. Jack Collender, Steve Davis, and Joe Frey generously contributed their time and effort to the mapping, data collecting and its analysis from part of the area as shown in Plate 1, inset. We thank Marty Morrison for running electron-probe analyses on andalusite and plagioclase in one specimen. Reviews by Paul Bateman, Frank Dodge, Phil Gans, Ben Page and Rich Schweickert helped clarify our writing, for which we are grateful.

REFERENCES

Ave Lallement, H. G., C. W. Weisenberg, and L. A. Standlee, Structural development of the Melones zone, northeastern California, Geol. Soc. Am. Abstr. Programs, 15, 372, 1977.

Bateman, P. C., Geologic map of the Blackcap Mountain quadrangle, Fresno County, California, Map GQ-428, U.S. Geol. Surv., Reston, Virginia, 1965.

Bateman, P. C. and L. D. Clark, Stratigraphic and structural setting of the Sierra Nevada batholith of California, Pac. Geol., 8, 79-89, 1974.

Bateman, P. C. and J. P. Eaton, Sierra Nevada batholith, Science, 158, 1407-1417, 1967.

Bateman, P. C. and J. G. Moore, Geologic map of the Mount Goddard quadrangle, Fresno and Inyo Counties, California, Map GQ-429, U.S. Geol. Surv., Reston, Virginia, 1965.

Bateman, P. C., A. J. Busacca, and W. N. Sawka, Cretaceous deformation in the western foothills of the Sierra Nevada, California, Geol. Soc. Am. Bull., 94, 30-42, 1983.

Bhattacharyya, T. and S. R. Paterson, Discussion: Timing and structural expression of the Nevada orogeny, Sierra Nevada, California, Geol. Soc. Am. Bull., 96, 1346-1347, 1985.

Brook, C. A., Stratigraphy and structure of the Saddelbag Lake roof pendant, Sierra Nevada, California, Geol. Soc. Am. Bull., 88, 321-334, 1977.

Brook, C. A., W. J. Nokleberg, and R. W. Kistler, Nature of the angular unconformity between the Paleozoic metasedimentary rocks and the Mesozoic metavolcanic ic rocks in the eastern Sierra Nevada, California, Geol. Soc. Am. Bull., 85, 571-576, 1974.

Chen, J. H. and J. G. Moore, Uranium-lead ages from the Sierra Nevada batholith, California, J. Geophys. Res., 87, 4761-4784, 1982.

Chen, J. H. and G. J. Wasserburg, Isotopic determination of Uranium in picomole and subpicomo equantities, Anal. Chem., 53, 2060-2067, 1981.

Dalmayrac, B. and P. Molnar, Parallel thrust and normal faulting in Peru and contraints on the state of stress, Earth Planet. Sci. Lett., 55, 473-481, 1981.

Day, H. W., E. M. Moores, and A. C. Tuminas, Structure and tectonics of the northern Sierra Nevada, Geol. Soc. Am. Bull., 96, 436-450, 1985.

DePaolo, D. J., A neodymium and strontium isotopic study of the Mesozoic calc-alkaline granitic batholiths of the Sierra Nevada and Peninsular ranges, California, J. Geophys. Res., 86, 10470-10488, 1981.

Dewey, J. F., Episodicity, sequence, and style at convergent plate boundaries, The Continental Crust and Its Mineral Deposits, edited by D. W. Strangeway, Geol. Assoc. Can. Spec. Pap. 20, 553-573, 1980.

DuBray, E. A., Geology of the igneous and metamorphic rocks in the Evolution-Goddard region of the Sierra Nevada, California, M.S. thesis, 123 pp., Stanford Univ., Stanford, Calif., 1977.

Elliott, D., Determination of finite strain and initial shape from deformed elliptical objects, Geol. Soc. Am. Bull., 81, 2221-2236, 1970.

Evernden, J. F., and R. W. Kistler, Chronology of emplacement of Mesozoic batholithic complexes in California and western Nevada, U.S. Geol. Surv. Prof. Pap. 623, 67 pp., 1970.

Fiske, R. S., Recognition and significance of pumice in marine pyroclastic rocks, Geol. Soc. Am. Bull., 80, 1-8, 1969.

Fiske, R. S., and E. D. Jackson, Orientation and growth of Hawaiin volcanic rifts: The effect of regional structure

and gravitational stresses, Proc. R. Soc. London. Ser. A, 239, 299-326, 1972.

Fiske, R. S. and T. Matsuda, Submarine equivalents of ash flows in the Tokiwa Formation, Japan, Am. J. Sci., 262, 76-106, 1964.

Fiske, R. S. and O. T. Tobisch, Paleogeographic significance of volcanic rocks of the Ritter Range pendant, central Sierra Nevada, California, Mesozoic Paleogeography of the Western United States, edited by D. G. Howell and K. A. McDougall, Soc. Econ. Paleontol. and Mineral., Pac. Coast Paleontol. Symp., 2, 209-222, 1978.

Fiske, R. S., O. T. Tobisch, R. W. Kistler, T. W. Stern, and M. Tatsumoto, Minarets caldera: a Cretaceous volcanic center in the Ritter Range pendant, central Sierra Nevada, Geol. Soc. Am. Abstr. Programs, 9, 275, 1977.

Fleuty, M. J., The description of folds, Proc. Geol. Assoc. London, 75, 461-492, 1964.

Gans, P. B. and E. L. Miller, Style of mid-Tertiary extension in east-central Nevada, Spec. Stud. Utah Geol. and Miner. Surv., 59, 107-160, 1983.

Gastil, R. G., A conceptual hypothesis for the relation of differing tectonic terranes to plutonic emplacement, Geology, 7, 542-544, 1979.

Grout, F. F., Scale models of structures related to batholiths, Am. J. Sci., 243-A, 260-284, 1945.

Hamilton, W. and W. B. Myers, The nature of batholiths, U.S. Geol. Surv. Prof. Pap. 554-C, 30 pp., 1967.

Hildreth, W., Gradients in silicic magma chambers: Implications for lithospheric magmatism, J. Geophys. Res., 86, 10153-10192, 1981.

Hildreth, W., R. E. Drake, and W. D. Sharp, Voluminous Late Pleistocene ash-flow and caldera complex in the Andes of central Chile, Geol. Soc. Am. Abstr. Programs, 13, 81, 1982.

Hsu, K. C., The characteristics of coaxial and non-coaxial strain paths, J. Strain Anal., 1, 216-222, 1966.

Huber, N. K. and C. D. Rinehart, Geologic map of the Devils Postpiles quadrangle, Sierra Nevada, California, Map GQ-437, U. S. Geol. Surv., Reston, Virginia, 1965.

Hussong, D. M. and S. Uyeda, Tectonic processes and the history of the Marianas arc: A synthesis of the results of the Deep Sea Drilling Project Leg 60, edited by M. Lee and R. Powell, Init. Rep. Deep Sea Drill. Proj., 60, 909-929, 1982.

Jaffey, A. H., K. F. Flynn, L. E. Glendenin, W. C. Bentley, and A. M. Essling, Precision measurement of the halflives and specific activities of 235U and 238U, Phys. Rev., C4, 1889-1906, 1971.

Karig, D. E., et al., Structure and Cenozoic evolution of the Sundra arc in the central Sumatra region, Geological and Geophysical Investigation of Continental Margins, edited by J. S Watkins, L. Montadert, and P. W. Dickerson, Am. Assoc. Pet. Geol. Mem. 29, 223-239, 1979.

Kistler, R. W., Structure and metamorphism in the Mono Craters quadrangle, Sierra Nevada, California, U.S. Geol. Surv. Bull., 1221E, 53 pp., 1966.

Kistler, R. W., and S. E. Swanson, Petrology and geochronology of metamorphosed volcanic rocks and a middle Cretaceous volcanic neck in the east-central Sierra Nevada, California, J. Geophys. Res., 86, 10489-10501, 1981.

Kistler, R. W., J. F. Evernden, and H. R. Shaw, Sierra Nevada Plutonic cycle, part I, origin of composite granitic batholiths, Geol. Soc. Am. Bull., 82, 853-868, 1971.

Krogh, T. E., A low-contamination method for hydrothermal decomposition of zircon an/d extraction of U and Pb for isotopic age determinations, Geochim. Cosmochim. Acta, 37/3, 485-494, 1973.

Lipman, P. W., The roots of ash flow calderas in western North America: windows into tops of granitic batholiths, J. Geophys. Res., 89, 8801-8841, 1984.

Lode, W. Versuche uber den Einfluss der mittleren Hauptspannung auf das fliessen des Metalle Eisen, Kupfer, und Nickel, Z. Phys., 36, 913-939, 1926.

Longiaru, S., Finite strain analysis and its impact on the interpretation of deformational history--An example from the eastern Sierra Nevada, Geol. Soc. Am. Abs. with Programs, 17, 646-647, 1985.

Marsh, B. D., On the mechanics of igneous diapirism, stoping and zone melting, Am. J. Sci., 282, 808-855, 1982.

Marsh, B. D., Reply: On the mechanics of igneous diapirism, stoping, and zone melting, Am. J. Sci., 284, 981-984, 1984.

Miller, E. L., P. B. Gans, and J. Garing, The Snake Range decollement: An exhumed mid-Tertiary ductile-brittle transition, Tectonics, 2, 239-263, 1983.

Molnar, P. and T. Atwater, Interarc spreading and cordilleran tectonics as alterna-

tives related to the age of subducted oceanic lithosphere, Earth Planet. Sci. Lett., 41, 330-340, 1978.

Moore, J. G., Geology of the Mount Pinchot quadrangle, southern Sierra Nevada, California, U.S. Geol. Surv. Bull., 1130, 152 pp., 1963.

Moores, E. M., Ultramafics and orogeny, with models of the U.S. Cordillera and the Tethys, Nature, 228, 837-842, 1970.

Moores, E. M. and H. W. Day, Overthrust model for the Sierra Nevada, Geology, 12, 416-419, 1984

Nadai, A., Theory of Flow and Fracture of Solids 2nd ed., Eng. Soc. Monogr., 705 pp., New York, McGraw-Hill, 1963.

Nokleberg, W. J., Stratigraphy and structure of the Strawberry Mine roof pendant, central Sierra Nevada, California, U.S. Geol. Surv. Prof. Pap., 1154, 18 pp., 1981.

Nokleberg, W. J. and R. W. Kistler, Paleozoic and Mesozoic deformations in the central Sierra Nevada, California, U.S. Geol. Surv. Prof. Pap., 1145, 24 pp., 1980.

Pitcher, W. S., The anatomy of a batholith, J. Geol. Soc. London, 135, 157-182, 1978.

Powell, C. McA., A morphological classification of rock cleavage, Tectonophysics, 58, 21-34, 1979.

Proffett, J. M., Jr., Cenozoic geology of the Yerington district, Nevada, and implications for the nature and origin of Basin and Range Faulting, Geol. Soc. Am. Bull., 88, 247-266, 1977.

Ramsay, J.G., Folding and Fracturing of Rocks, 568 pp., New York, McGraw-Hill, 1967.

Ricci, M. P., E. M. Moores, K. L. Verosub, and J. S. McClain, Geologic and gravity evidence for thrust emplacement of the Smartville Ophiolite, Tectonics, 4, 539-546, 1985.

Rinehart, C. D. and D. C. Ross, Geology and mineral deposits of the Mount Morrison quadrangle, Sierra Nevada, California, U.S. Geol. Surv. Prof. Pap., 385, 106 pp., 1964.

Russell, S. J. and W. J. Nokleberg, Superimposition and timing of deformations in the Mount Morrison roof pendant and in the central Sierra Nevada, California, Geol. Soc. Am. Bull., 88, 335-345, 1977.

Saleeby, J., Polygenetic ophiolite belt of the California Sierra Nevada, geochronological and tectonostratigraphic development, J. Geophys. Res., 87, 1802-1824, 1982.

Saleeby, J. B. and Sharp, W. D., Chronology of the structural and petrologic development of the southwest Sierra Nevada foothills, California, part I, Geol. Soc. Am. Bull., 91, 317-320, 1980.

Saleeby, J.B. et al., Ocean-continent transect, Corridor C2, Monterey Bay offshore to the Colorado Plateau, scale 1:500,000, 2 sheets and explanatory text, Map Chart Ser. Geol. Soc. Am., Boulder, Colo., 1985.

Sams, D. B., U/Pb zircon geochronology, petrology and structural geology of the crystalline rocks of the southernmost Sierra Nevada and Tehachapi Mountains, Kern County, California, Ph.D. thesis, 211 pp., Calif. Inst. of Technol., Pasadena, 1985.

Schweickert, R. A. and D. S. Cowan, Early Mesozoic tectonic evolution of the western Sierra Nevada, California, Geol. Soc. Am. Bull., 86, 1329-1336, 1975.

Schweickert, R. A., G. R. Fisher, and M. W. Lahren, Structural and tectonic history of the Saddlebag Lake Pendant (SLP), eastern Sierra Nevada, California, Geol. Soc. Am. Abstr. Programs, 16/5, p. 332, 1984a.

Schweickert, R. A., N. C. Bogen, G. H. Girty, R. E. Hanson, and C. Merguerian, Timing and structural expression of the Nevadan orogeny, Sierra Nevada, California, Geol. Soc. Am. Bull., 95, 967-979, 1984b.

Silver, L. T., The relationship between radioactivity and discordance in zircons, Nuclear Geophysics, N.A.S.- N.R.C. Publ., 1075, 34-39, 1964.

Stern, T. W., P. C. Bateman, B. A. Morgan, M. F. Newell, and D. L. Peck, Isotopic U-Pb ages of zircon from the granitoids of the central Sierra Nevada, California, U.S. Geol. Surv. Prof. Pap., 1185, 17 pp., 1981.

Tobisch, O. T., Development of cleavage in lapilli-bearing volcaniclastic rock, Tectonophysics, 109, 309-335, 1984.

Tobisch, O. T. and R. S. Fiske, Significance of conjugate folds and crenulations in the central Sierra Nevada, California, Geol. Soc. Am. Bull., 87, 1411-1420, 1976.

Tobisch, O. T. and R. S. Fiske, Repeated parallel deformation in part of the eastern Sierra Nevada, California, and its implications in the dating of structural events, J. Struct. Geol., 4, 177-195, 1982.

Tobisch, O. T., R. S. Fiske, S. Sacks, and D. Taniguchi, Strain in metamorphosed volcaniclastic rocks and its bearing on

the evolution of orogenic belts, Geol. Soc. Am. Bull., 88, 23-40.

Tobisch, O. T., J. B. Saleeby, and R. S. Fiske, Extensional model for intra-arc deformation of metavolcanic rocks in the eastern Sierra Nevada, California, Geol. Soc. Am. Abstr. Programs, 17/6, 413, 1985.

Turner, F. J., Metamorphic Petrology: Mineralogical, Field, and Tectonic Aspects, 524 pp., New York, McGraw Hill, 1981.

Uyeda, S., Subduction zones: An introduction to comparative subductology, Tectonophysics, 81, 133-159, 1982.

Uyeda, S. and H. Kanamori, Back-arc opening and the mode of subduction, J. Geophys. Res., 84, 1049-1061, 1979.

Von Heune, R., et al., Leg 67: The Deep Sea Drilling Project Mid-Trench transect off Guatemala, Geol. Soc. Am. Bull., 91, part I, 421-432, 1980.

Wernicke, B., Low angle normal faults in the Basin and Range province: Nappe tectonics in an extending orogen, Nature, 291, 645, 1981.

Wetherill, G. W., Discordant uranium-lead ages, 1, Eos Trans. AGU, 37, 320-326, 1956.

Wood, D. S., Patterns and magnitudes of natural strain in rocks, Philos. Trans. R. Soc. London, Ser. A, 274, 373-382, 1973.

York, D., Least-squares fitting of a straight line, Can. J. Phys., 44, 1079-1086, 1966.

R. S. Fiske, National Museum of Natural History NHB-119, Smithsonian Institution, Washington, D. C., 20560.

J. B. Saleeby, Division of Geological and Planetary Sciences, California Institute of Technology, Pasadena, CA, 91125.

O. T. Tobisch, Earth Science Department, Applied Science Building, University of California, Santa Cruz, CA, 95064.

(Received May 8, 1985;
revised October 7, 1985;
accepted October 8, 1985)